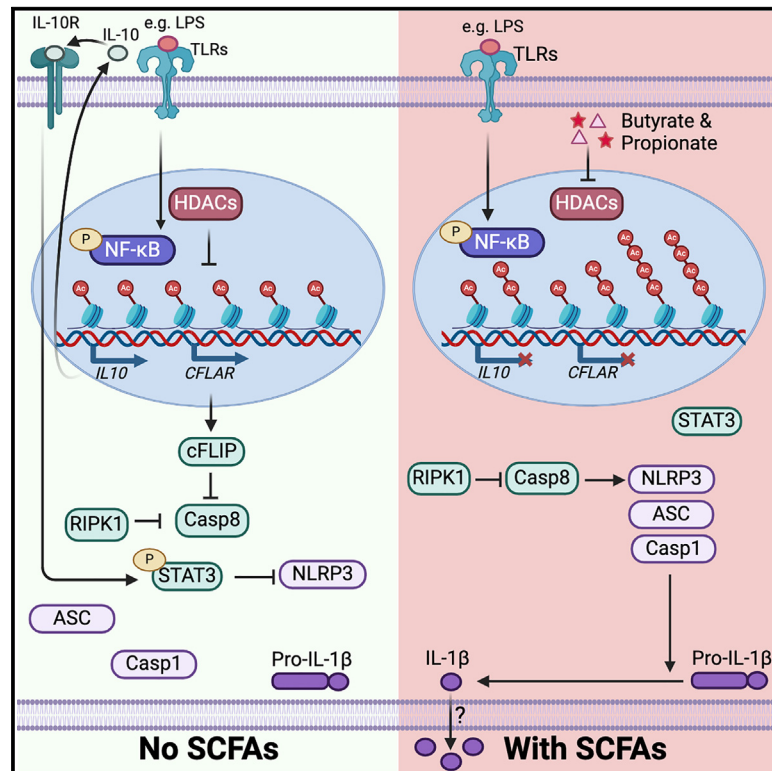# Butyrate and propionate are microbial danger signals that activate the NLRP3 inflammasome in human macrophages upon TLR stimulation

Graphical abstract

Authors

Wei Wang, Alesja Dernst,
Bianca Martin, ..., Sergi Cuartero,
Eicke Latz, Matthew S.J. Mangan

Correspondence

eicke.latz@drfz.de (E.L.),
matthew.mangan@ukbonn.de (M.S.J.M.)

In brief

Latz et al. show that the bacterially derived metabolites short-chain fatty acids (SCFAs) are sensed as danger signals under inflammatory conditions through the NLRP3 inflammasome. Mechanistically, SCFAs inhibited HDACs, causing alterations in transcription that resulted in the loss of cFLIP and IL-10 expression, leading to caspase-8-dependent NLRP3 inflammasome activation.

Highlights

- SCFAs activate the NLRP3 inflammasome under inflammatory conditions

- SCFAs inhibit HDAC activity, altering the LPS-dependent transcriptome

- This causes loss of cFLIP and IL-10 expression, triggering NLRP3 activation

- SCFA-mediated NLRP3 activation causes hyperactivation but not pyroptosis

CellPress

Article

Butyrate and propionate are microbial danger signals that activate the NLRP3 inflammasome in human macrophages upon TLR stimulation

Wei Wang,[1,6,10] Alesja Dernst,[1,10] Bianca Martin,[1] Lucia Lorenzi,[2] Maria Cadefau-Fabregat,[2] Kshiti Phulphagar,[1] Antonia Wagener,[1] Christina Budden,[1] Neil Stair,[3,4] Theresa Wagner,[1] Harald Färber,[5] Andreas Jaensch,[5] Rainer Stahl,[1] Fraser Duthie,[1] Susanne V. Schmidt,[1] Rebecca C. Coll,[6] Felix Meissner,[1] Sergi Cuartero,[2] Eicke Latz,[1,7,8,9,11,12,*] and Matthew S.J. Mangan[1,7,11,*]

[1]Institute of Innate Immunity, University Hospital Bonn, University of Bonn, 53127 Bonn, Germany
[2]Josep Carreras Leukemia Research Institute (IJC), 08916 Badalona, Barcelona, Spain
[3]Institute for Genetics, CECAD Research Center, University of Cologne, 50931 Cologne, Germany
[4]Cologne Excellence Cluster on Cellular Stress Responses in Aging-associated Diseases (CECAD), University of Cologne, 50931 Cologne, Germany
[5]Institute for Hygiene and Public Health, University Hospital Bonn, University of Bonn, 53127 Bonn, Germany
[6]Wellcome-Wolfson Institute for Experimental Medicine, Queen's University Belfast, Belfast BT9 7BL, UK
[7]German Center for Neurodegenerative Diseases, 53127 Bonn, Germany
[8]Department of Infectious Diseases & Immunology, UMass Medical School, Worcester, MA 01605, USA
[9]Deutsches Rheuma Forschungszentrum Berlin (DRFZ), 10117 Berlin, Germany
[10]These authors contributed equally
[11]These authors contributed equally
[12]Lead contact
*Correspondence: eicke.latz@drfz.de (E.L.), matthew.mangan@ukbonn.de (M.S.J.M.)
https://doi.org/10.1016/j.celrep.2024.114736

SUMMARY

Short-chain fatty acids (SCFAs) are immunomodulatory compounds produced by the microbiome through dietary fiber fermentation. Although generally considered beneficial for gut health, patients suffering from inflammatory bowel disease (IBD) display poor tolerance to fiber-rich diets, suggesting that SCFAs may have contrary effects under inflammatory conditions. To investigate this, we examined the effect of SCFAs on human macrophages in the presence of Toll-like receptor (TLR) agonists. In contrast to anti-inflammatory effects under steady-state conditions, we found that butyrate and propionate activated the NOD-, LRR-, and pyrin domain-containing protein 3 (NLRP3) inflammasome in the presence of TLR agonists. Mechanistically, these SCFAs prevented transcription of FLICE-like inhibitory protein (cFLIP) and interleukin-10 (IL-10) through histone deacetylase (HDAC) inhibition, triggering caspase-8-dependent NLRP3 inflammasome activation. SCFA-driven NLRP3 activation was potassium efflux independent and did not result in cell death but rather triggered hyperactivation and IL-1β release. Our findings demonstrate that butyrate and propionate are bacterially derived danger signals that regulate NLRP3 inflammasome activation through epigenetic modulation of the inflammatory response.
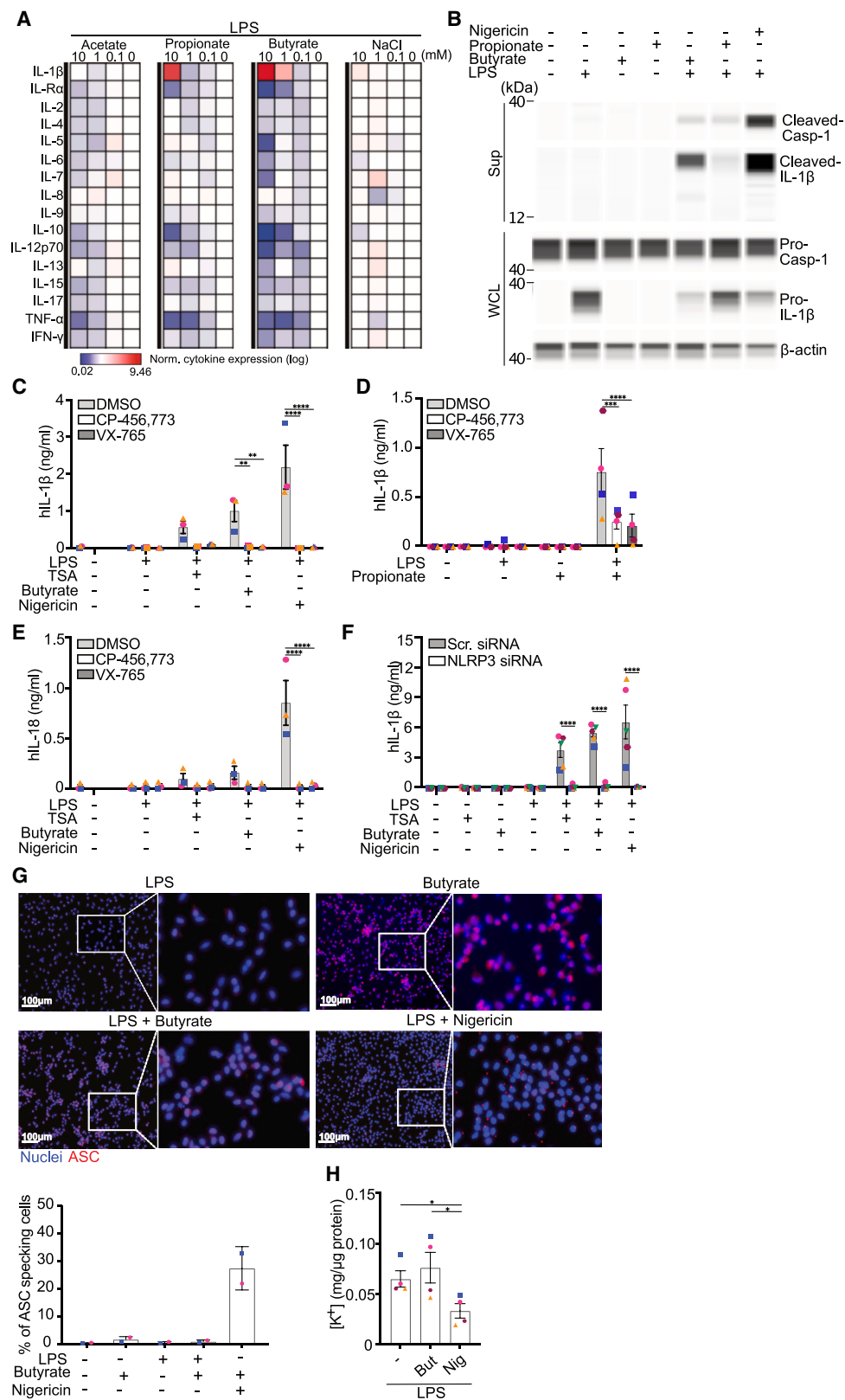
INTRODUCTION

Short-chain fatty acids (SCFAs), including acetate, propionate, and butyrate, are generated at high concentrations by the microbiota through fermentation of dietary fiber.[1] This occurs in the intestine, where concentrations can range from 10 to 90 mM at a ratio of 3:1:1 acetate:propionate:butyrate, as well as in the periodontal pockets in the mouth.[1,2] Under steady-state conditions, SCFAs play a crucial role in maintaining gut homeostasis by supporting the integrity of the intestinal epithelial barrier and modulating the function of immune cells. SCFAs mediate these effects through multiple mechanisms: activation of G protein-coupled receptors and olfactory receptors, inhibi-

tion of histone deacetylase (HDAC) activity, or as a fuel source.[3–5] One notable example is their effect on intestinal macrophages, where butyrate, through epigenetic modification, triggers differentiation of monocytes to macrophages and imprints an anti-inflammatory, antimicrobial transcriptional program.[6]

Due to their action as immune modulators, SCFAs have been studied as a potential therapy for intestinal inflammatory disorders, including IBD.[7] IBD is characterized by a breakdown of the intestinal epithelial cell barrier, resulting in ongoing inflammation that is thought to underlie the pathology of the condition.[7] However, it remains unclear whether SCFAs are beneficial or detrimental for IBD, as fiber, which enables SCFA

(legend on next page)

production, is poorly tolerated by IBD patients in some cases.[8,9] This intolerance is partially attributed to the type of fiber ingested,[10] but diets that increase the level of SCFAs do not always have beneficial effects.[11]

The role of inflammation in IBD has suggested that drugs targeting inflammatory cytokines involved in the would have therapeutic potential. However, drugs targeting tumor necrosis factor alpha (TNF-α), interleukin-12 (IL-12), or IL-6 have been unable to completely reverse the IBD phenotype.[12–14] Subsequently, the NLRP3 inflammasome, which triggers secretion of IL-1β and IL-18, has emerged as a new potential target in the treatment of IBD. Notably, people harboring hyperactivating NLRP3 mutations have an increased risk of ulcerative colitis and IBD.[15,16] This is less clear in two murine models of colitis, dextran sulfate sodium (DSS) and 2,4,6-trinitrobenzenesulfonic acid, where NLRP3 has been suggested to be both detrimental and protective in the disease.[17–20] Furthermore, the ablation of caspase-1 rescued the spontaneous colitis that occurs in the IL-10-deficient murine model.[21] The variations in the results likely reflect the complex etiology of IBD and differences arising from disparities in genetic background, housing conditions, and microbiota composition. Perhaps the most relevant result, then, is that CP-456,773 (also called CRID3 or MCC950) mitigated DSS colitis in littermate controls with the same genetic background,[17] indicating that NLRP3 is a relevant target for treatment of IBD.

RESULTS

Butyrate and propionate decrease the LPS-driven cytokine response but trigger IL-1β release

To investigate the impact of SCFAs on the inflammatory response in human macrophages, we incubated human monocyte-derived macrophages (hMDMs), differentiated with granulocyte-macrophage colony-stimulating factor (GM-CSF), with lipopolysaccharide (LPS) in the presence or absence of the SCFAs butyrate, propionate, or acetate. Compared to LPS, co-incubation of LPS with SCFAs decreased secretion of most LPS-dependent cytokines, including IL-10, IL-12p40, and IL-6 (Figure 1A). Butyrate had the strongest effect, altering cytokine secretion at 1 mM, while propionate exhibited a moderate effect, and acetate had almost no effect. However, in contrast to most

of the assessed cytokines, co-incubation of LPS with butyrate and propionate triggered release of IL-1β, a key pro-inflammatory cytokine (Figure 1A). Maximal release of IL-1β occurred at 4 mM butyrate, although it was evident at a dose as low as 1 mM (Figure S1A) and was released from 6 h onward (Figure S1B). We then assessed monocytes, which, in contrast to macrophages, release IL-1β in response to LPS alone without needing a secondary trigger.[22] Markedly, butyrate and propionate triggered IL-1β release following co-incubation with LPS and butyrate at a concentration of LPS that did not elicit IL-1β release alone (Figure S1C). This demonstrates that SCFAs generally activate IL-1β release from myeloid cells in the presence of LPS.

SCFA-mediated IL-1β release is dependent on the NLRP3 inflammasome

A key mechanism driving IL-1β release is activation of an inflammasome complex. Among these, NLRP3 is the most notable, triggering inflammasome formation in response to a diverse range of cell stresses.[23] Therefore, we assessed hallmarks of inflammasome activation, cleavage of IL-1β and caspase-1, in LPS-primed hMDMs incubated with either SCFA. Nigericin, a canonical NLRP3 activator, was included as a control. Notably, butyrate and propionate resulted in cleavage and release of IL-1β and caspase-1, similar to nigericin (Figure 1B), indicating that they trigger inflammasome activation. Furthermore, IL-1β cleavage was evident when butyrate was co-incubated with Pam3CSK4 (Toll-like receptor 2 [TLR2]), flagellin (TLR5), and R848 (TLR7/8), demonstrating that activation of any TLR in the presence of butyrate is sufficient for NLRP3 activation (Figures S1C and S1D). To investigate whether SCFA-mediated IL-1β release by activating the NLRP3 inflammasome, we inhibited NLRP3 with CP-456,773 (also called MCC-950 and CRID3) or caspase-1 with VX-765 and stimulated hMDMs with butyrate or propionate. Both VX-765 and CP-456,773 inhibited IL-1β release and cleavage mediated by butyrate (Figures 1D and S1C), propionate (Figure 1F), and nigericin (Figure 1F). Furthermore, both inhibitors blocked butyrate- and nigericin-mediated IL-18 release. Collectively, this indicates that both SCFAs activate the NLRP3 inflammasome. To confirm this, we knocked down NLRP3 in hMDMs (Fig. S1D). Compared to

---

Figure 1. SCFAs decrease LPS-induced cytokine secretion but trigger NLRP3 inflammasome-dependent IL-1β release

(A) Heatmap of cytokines measured from cell-free supernatant (sup) from hMDMs stimulated with LPS (1 ng/mL, 16 h) with or without acetate, propionate, or butyrate and normalized to LPS and NaCl. $n = 6$.

(B) hMDMs incubated with butyrate (5 mM), propionate (10 mM), or nigericin (10 μM) with LPS (1 ng/mL). IL-1β and caspase-1 cleavage assessed from sup or whole-cell lysate (WCL) by WES. Representative of $n = 2$.

(C) IL-1β release from sup from hMDMs treated with butyrate (10 mM), Trichostatin A (TSA) (0.5 μM), and LPS (1 ng/mL) or LPS (1 ng/mL, 3 h) and nigericin (10 μM, 1.5 h) with or without CP-456,773 (2 μM, 30 min) or VX-765 (40 μM, 30 min).

(D) IL-1β release measured from sup from hMDMs treated with propionate (10 mM) and LPS (1 ng/mL) with or without CP-456,773 (2 μM, 30 min) or VX-765 (40 μM, 30 min).

(E) IL-18 release from hMDMs treated as in (C).

(F) IL-1β release from NLRP3- or scrambled siRNA-treated hMDMs incubated with butyrate (10 mM) or TSA (0.5 μM) and LPS (1 ng/mL) for 16 h or nigericin (10 μM, 1.5 h).

(G) Fluorescence imaging of apoptosis-associated speck-like protein containing a CARD (ASC) (red) and nuclei (blue) in hMDMs treated with LPS and butyrate or nigericin in the presence of VX-765. Quantitation of ASC specks is shown for 4 images per condition.

(H) Cellular potassium from hMDMs treated as in (D) and analyzed by ICP-MS; representative of $n = 4$.

Mean ± SEM are shown; each dot represents one donor. *$p < 0.05$, **$p < 0.01$, ***$p < 0.001$, ****$p < 0.0001$ by two-way ANOVA with Šídák's multiple-comparisons test.

A

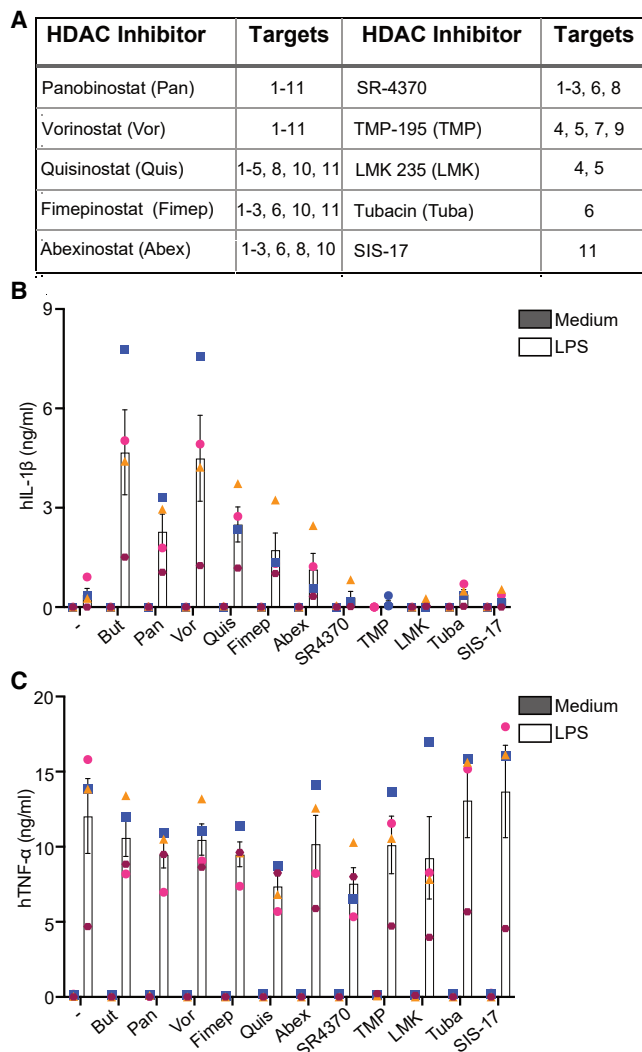| HDAC Inhibitor	Targets	HDAC Inhibitor	Targets
Panobinostat (Pan)	1-11	SR-4370	1-3, 6, 8
Vorinostat (Vor)	1-11	TMP-195 (TMP)	4, 5, 7, 9
Quisinostat (Quis)	1-5, 8, 10, 11	LMK 235 (LMK)	4, 5
Fimepinostat (Fimep)	1-3, 6, 10, 11	Tubacin (Tuba)	6
Abexinostat (Abex)	1-3, 6, 8, 10	SIS-17	11

B

C

Figure 2. Inhibition of HDACs 1–3 and 10 enables NLRP3 activation in response to TLR stimulation
(A) HDAC inhibitors and their specificities. hMDMs were treated with HDAC inhibitors with or without LPS (1 ng/mL, 16 h). Concentrations used were as follows: butyrate (10 mM), Pan (1 μM), Vor (1 μM), quisinostat (Quis) (0.2 μM), fimepinostat (Fimep) (0.1 μM), abexinostat (Abex) (0.1 μM), SR4370 (4 μM), TMP-195 (TMP) (0.3 μM), LMK 235 (LMK) (20 nM), tubacin (Tuba) (50 nM), and SIS-17 (1 μM).
(B and C) IL-1β release (B) and TNF-α secretion (C) measured from sup. Mean ± SEM are shown; each dot represents one donor.

the scrambled control, NLPR3 knockdown ablated butyrate-, Trichostatin A (TSA)-, and nigericin-mediated IL-1β release (Figure 1E) but had no effect on TNF-α secretion (Figure S1E), confirming that both butyrate and propionate activate NLRP3. It was surprising that we observed NLRP3 activation, as butyrate and propionate ablated expression of nuclear factor κB (NF-κB)-inducible genes, which should include *NLRP3* and *IL1B*. Consistent with our other results, we observed a decrease in both NLRP3 and IL-1β mRNA at 16 h (Fig. S1H). However, NLRP3 or pro- IL-1β protein levels did not change between the LPS

and LPS and butyrate conditions (Figure S1I), demonstrating that the drop in transcription did not affect the amount of either protein.

NLRP3 activation can also trigger aggregation of the adapter apoptosis-associated speck-like protein containing a CARD (ASC), resulting in formation of the ASC "speck". However, in comparison to nigericin, almost no ASC specks were observed in hMDM response to butyrate (Figure 1H), suggesting that these are not required for the butyrate-driven NLRP3 response. The absence of ASC speck formation was reminiscent of the alternative pathway of activation observed in human monocytes in response to prolonged exposure to LPS.[24] Unlike the majority of NLRP3 activators, alternative NLRP3 activation does not trigger potassium efflux. Therefore, we measured potassium levels in the hMDMs following stimulation with LPS, LPS and butyrate, or LPS and nigericin using inductively coupled plasma mass spectrometry (ICP-MS). LPS and butyrate did not cause a decrease in cellular potassium compared to the hMDMs treated with LPS alone (Figure 1I), while there was a marked decrease in response to nigericin (Figure 1I). This demonstrates that butyrate-driven NLRP3 activation does not require potassium efflux.

Inhibition of HDACs 1–3, 8, and 10 is sufficient to trigger NLRP3-dependent IL-1β release

SCFAs mediate many of their functions through the inhibition of HDAC activity.[25] The propensity of SCFAs to activate NLRP3 correlated with their effectiveness as HDAC inhibitors, as butyrate and propionate, but not acetate, inhibit HDACs.[26] Furthermore, TSA, a pan-HDAC inhibitor, triggered NLRP3-dependent IL-1β release, suggesting that this could be the mechanism through which SCFAs activate NLRP3. We confirmed this with two other pan-HDAC inhibitors, panobinostat (Pan) and vorinostat (Vor), which both triggered IL-1β release from LPS-primed hMDMs (Figure 2B). To determine which HDAC(s) were required, we assessed HDAC expression in hMDMs and knocked down the expressed HDACs (Figure S2A). However, individual knockdown of any of the HDACs tested did not trigger IL-1β release in response to LPS alone (Figure S2B) and did not alter TNF-α secretion (Figure S2B). This suggested that the HDACs regulating NLRP3 activation were redundant, consistent with HDACs having overlapping function.[27] Therefore, we used HDAC inhibitors with different specificities to determine which HDACs needed to be inhibited to activate NLRP3. Inhibitors targeting a combination of HDACs 1–3 and 10 could all mediate IL-1β release in the presence of LPS (Figure 2B), but did not perturb secretion of TNF-α (Figure 2C), demonstrating that inhibition of HDAC activity activates NLRP3 under inflammatory conditions. To determine whether HDAC inhibition is the pathway used by SCFAs to activate NLRP3, we incubated LPS-primed hMDMs with Pan or Vor alone or in combination with butyrate. Notably, butyrate did not increase IL-1β release when added in addition to Pan or Vor (Figure S2C), providing a strong indication that they activate NLRP3 through the same pathway.

Butyrate and propionate modulate the LPS-driven gene expression profile

Activation of NLRP3 by butyrate and propionate required the inhibition of HDAC activity, which, along with a relatively long

incubation period, suggested that it required changes in transcription. Therefore, we assessed the effect of SCFAs on the LPS-mediated transcriptome in hMDM using RNA sequencing (RNA-seq). TSA was included to define the effect of HDAC inhibition on the LPS response.

The principal-component analysis demonstrated that butyrate clustered with TSA (Figure 3A), and their gene signatures almost completely overlapped (Figure S3A). Propionate had a similar but weaker effect compared to butyrate and TSA (Figure 3A), also showing an overlapping signature with butyrate (Figure S3B), while acetate had a minimal effect (Figure 3A). Consistent with our cytokine data, butyrate and TSA reversed the effect of the LPS-dependent transcriptional signature, decreasing expression of genes decreased by LPS or vice versa (Figure 3B). Notably, in spite of histone acetylation being associated with increased gene transcription, butyrate, TSA, and propionate decreased transcription of a similar number of genes as they increased (Figure 3C). We examined these using a gene set enrichment analysis (GSEA) on hallmark gene sets and found that the genes decreased by butyrate, TSA, and, to a lesser extent, propionate, were enriched for terms associated with the inflammatory response, including "inflammatory cytokine response" and "interferon" (Figure 3D). In contrast, the few terms that were significantly enriched in upregulated genes were not consistently identified among the three treatments, indicating that no specific pathways were activated by SCFAs (Figure 3D). The correlation between the enriched pathways from SCFAs and TSA suggested that the primary effect of SCFAs on the LPS-driven gene signature was due to HDAC inhibition.

The overlap in gene changes between the SCFAs and TSA suggested that SCFA-mediated HDAC inhibition altered transcription of inflammatory and interferon-related genes by modifying histone acetylation. We first confirmed that incubating hMDMs with butyrate increased total levels of acetylated lysine 27 on histone H3 (H3K27ac), a hallmark of active transcription at enhancers and promoters (Figure S3C). We then delineated the genomic distribution of the increase in H3K27ac by performing chromatin immunoprecipitation sequencing (ChIP-seq). Consistent with the hyperacetylation observed by immunoblot, butyrate increased the number of the total called peaks by almost 4-fold (Figure S3D) and caused a general increase in H3K27ac both at promoters and at intergenic peaks (Figure S3E). However, the increase in H3K27ac at gene promoters was distributed unevenly and correlated significantly with the changes in gene expression caused by butyrate (Figure 3E). Genes with the lowest increase in acetylation tended to show decreased transcription and vice versa (Figure 3F). GSEA showed that pathways enriched among downregulated genes were also significantly enriched among genes with a low acetylation increase and included pathways such as "interferon," "inflammatory response," or "NF-κB" (Figure 3G). Genes belonging to these pathways had less of an acetylation increase than the average of all genes or specific subsets with high hyperacetylation (Figure 3H). Transcription factor (TF) binding motif enrichment of downregulated gene promoters in RNA-seq (butyrate + LPS vs. LPS) and the 10% of genes with the lowest H3K27ac increase (butyrate + LPS vs. LPS) showed a significant enrichment for interferon-associated TFs (Figure 3I). In contrast, enrichment

for TF binding motifs from upregulated genes or those with the most increased H3K27ac showed general promoter-binding TFs and no consistent pathways (Figure S3F).

To determine whether the changes seen on the RNA level reflected changes in protein levels, we performed proteomics on hMDMs incubated with LPS with or without butyrate or TSA. While we identified considerably fewer differentially regulated proteins compared to the RNA-seq results (Figure S3G), butyrate and TSA still clustered together by multidimensional scaling plot (Figure S3H) and hierarchical clustering (Figure S3I). GSEA showed that pathways similar to those in the RNA-seq data were altered, demonstrating that the changes observed in the RNA-seq data were also occurring on the protein level (Figure S3J).

SCFAs decrease expression of cFLIP and XIAP

The butyrate- and TSA-dependent decrease in genes involved in the inflammatory response was particularly interesting. Previous studies have shown that inhibition of the NF-κB signaling pathway, following engagement of a TLR, results in caspase-8 activation,[28,29] which can, in some cases, lead to activation of the NLRP3 inflammasome.[30] Analysis of the RNA-seq dataset revealed that butyrate and TSA decreased expression of two key regulators of caspase-8, cFLIP (*CFLAR*) and X-linked inhibitor of apoptosis protein (XIAP) (Figure 4A). Consistent with the global correlation between gene expression and H3K27ac changes induced by butyrate, both the *CFLAR* and *XIAP* genes were among the 10% with the lowest increase in promoter acetylation (Figure 4B). We confirmed the decrease in expression by qPCR, which showed that butyrate and TSA decreased transcripts of both genes regardless of LPS pre-treatment (Figure 4C).

cFLIP can be transcribed in multiple isoforms, a long isoform (cFLIP$_L$) or two short isoforms (cFLIP$_R$ and cFLIP$_S$).[31] Consistent with alterations on the RNA level, expression of both the long and short isoforms of cFLIP were reduced in the presence of butyrate (Figure S4A) and propionate (Figure S4B). However, neither SCFA noticeably reduced XIAP protein levels (Figure S4B). Correlating cFLIP and XIAP expression with IL-1β release over time revealed that cFLIP$_L$ expression was lost as early as 4 h (Figures 4D and 4E), correlating with the time we required for IL-1β release (Figure 4F). In contrast, XIAP decreased across the time course but was not completely absent until 12–16 h (Figures 4D and 4E). To ensure that loss of cFLIP was due to changes in gene expression, we assessed cFLIP degradation. However, inhibitors of the proteasome had no effect on cFLIP protein level in this time frame (Figure S4C).

Butyrate-dependent ablation of cFLIP is required for NLRP3 inflammasome activation

The correlation between IL-1β release and the loss of cFLIP expression suggested that it was required for NLRP3 activation. To investigate this, we expressed cFLIP in hMDMs using lentiviral transduction, resulting in exogenous cFLIP expression at a level comparable to the endogenous expression in the absence of butyrate (Figure 4G). Exogenous expression of cFLIP, but not vector alone, prevented LPS and butyrate-mediated IL-1β release but had no effect on activation of the NLRC4
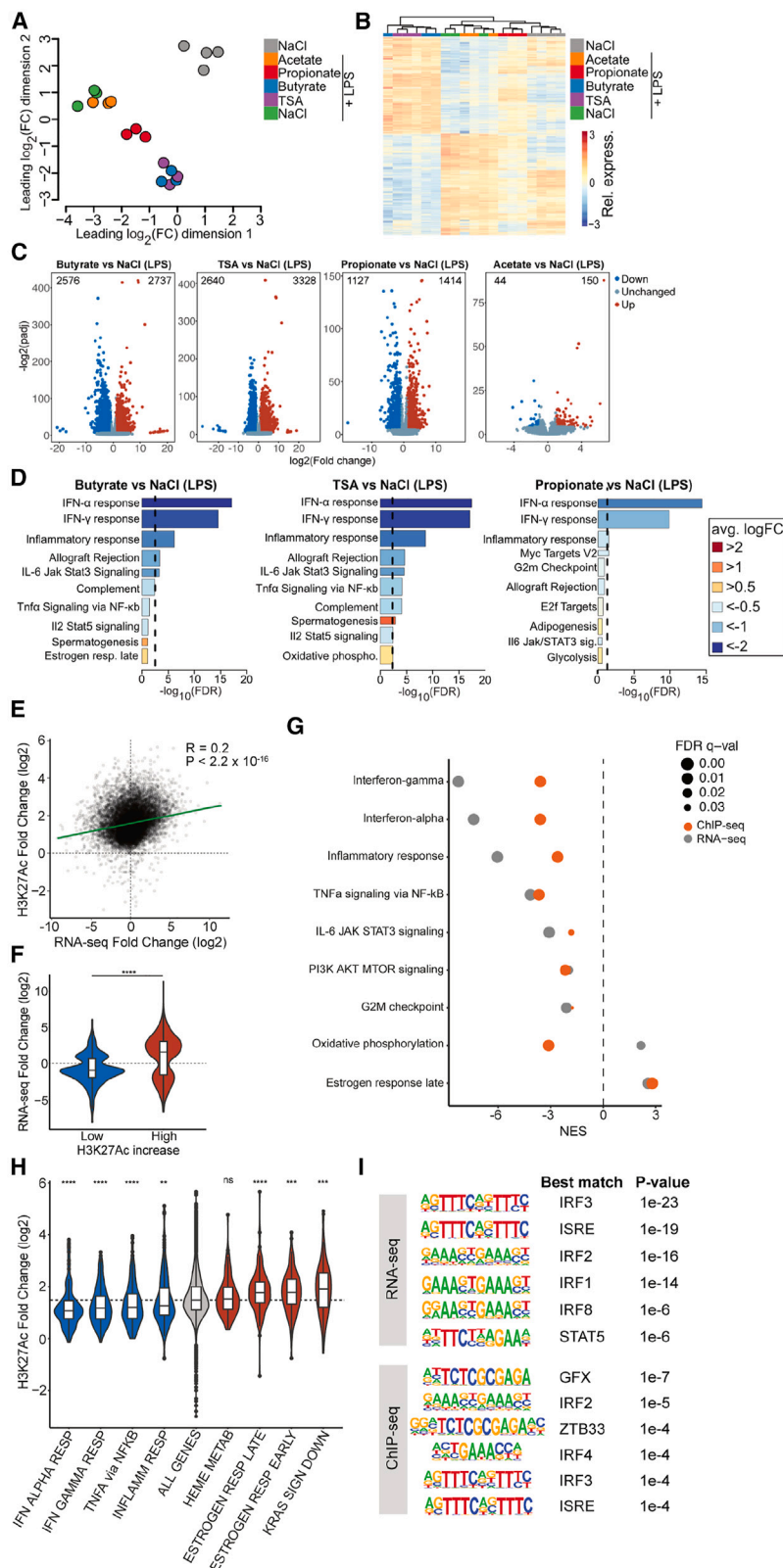
Shown is RNA-seq analysis of hMDMs treated with either NaCl, acetate, propionate, or butyrate (all 10 mM) or TSA (0.5 μM) with LPS (1 ng/mL).

(A) Multidimensional scaling plot visualizing the relationship between the samples. $n = 3–4$.

(B) Heatmap depicting relative expression values of transcripts significantly changed in LPS + butyrate vs. LPS + NaCl comparison, scaled by row.

(C) Volcano plots of genes altered by incubation with SCFAs or TSA compared to LPS alone. Significant up- and downregulated genes (adjusted $p < 0.05$ and absolute log2(fold change) > 1) are shown in red and blue, respectively.

(D) Gene set enrichment analysis (GSEA) performed based on the Molecular Signatures Database, using the hallmark gene sets. Plots show the top 10 hallmark gene sets. Bars are colored by average log2(fold change) ($log_2(FC)$). Bar width represents the number of genes in the respective gene set. A dashed line indicates the adjusted p value threshold.

(E) Correlation between the FC of differential H3K27ac signals at promoters (ChIP-seq) and the FC of differential gene expression (RNA-seq) comparing butyrate + LPS vs. LPS alone. Correlation was tested by Spearman correlation coefficient (R).

(F) Distribution of the RNA-seq FC between butyrate + LPS vs. LPS alone for genes with the 10% lowest and 10% highest increase in H3K27ac ChIP-seq signal at promoters.

(G) Normalized enrichment score from GSEA of hallmark gene sets using either RNA-seq or H3K27ac ChIP-seq signal for the comparison LPS + butyrate vs. LPS alone. Only gene sets showing significance in both datasets (false discovery rate q < 0.05) are shown.

(H) FC in H3K27ac signal at promoters of genes belonging to gene sets negatively and positively enriched (by GSEA), shown in blue and red, respectively. Gray shows values for all genes.

(I) Motif enrichment analyses for downregulated genes (RNA-seq) and the 10% of promoters with the lowest H3K27ac increase (ChIP-seq) comparing butyrate + LPS vs. LPS alone.

*$p < 0.05$, **$p < 0.01$, ***$p < 0.001$, ****$p < 0.0001$ by Wilcoxon's test.
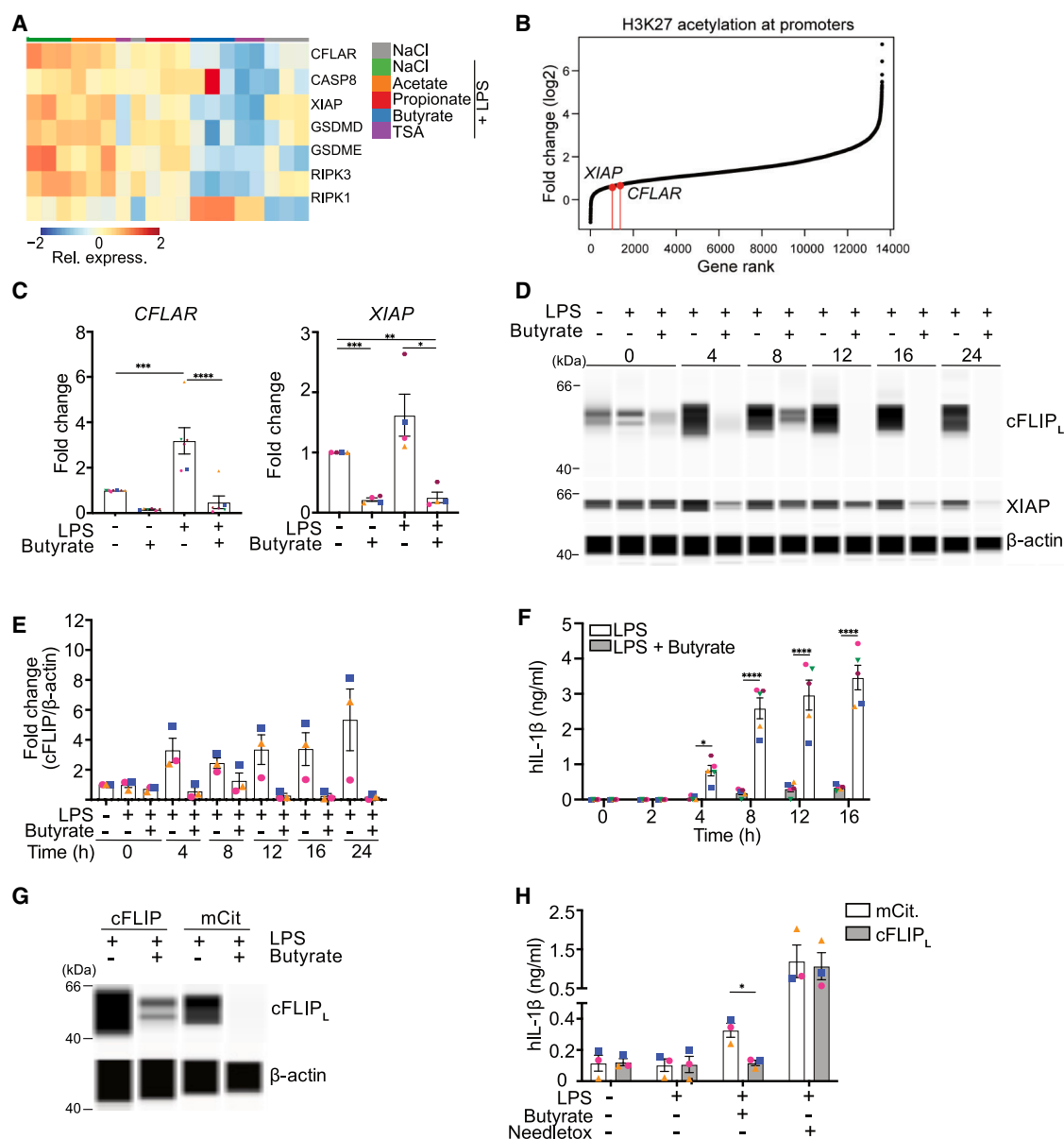
Figure 4. Butyrate-mediated decrease in cFLIP expression is required for NLRP3 inflammasome activation

(A) Expression of cell death-related gene expression values of transcripts significantly changed in LPS + butyrate compared to LPS + NaCl, scaled by row (*n* = 3).

(B) Ranking of all genes ordered by the FC in H3K27ac signal in LPS + butyrate-treated samples.

(C) *CFLAR* and *XIAP* expression assessed by qPCR; *n* = 6. hMDMs were treated with LPS (1 ng/mL) with or without butyrate (10 mM).

(D and E) cFLIP_L and XIAP assessed by WES (D) and quantified (E); representative of *n* = 4.

(F) IL-1β release measured from sup from (D).

(G) hMDMs were transduced with cFLIP_L or vector alone and stimulated with LPS (1 ng/mL) and/or butyrate (5 mM, 16 h) or Needle-Tox (1 μg/mL Needle-Tox, 1 μg/mL protective antigen [PA], 1.5 h). cFLIP expression assessed by WES, representative of *n* = 3.

(H) IL-1β release measure from sup.

Mean ± SEM are shown, each dot represents one donor. *$p < 0.05$, **$p < 0.01$, ***$p < 0.001$, ****$p < 0.0001$ by either one way ANOVA with Tukey test (C) or two-way ANOVA with Šídák's multiple-comparisons test (F and G).

inflammasome by its activator Needle-Tox (Figure 4H), demonstrating that loss of cFLIP was required for NLRP3 activation. To determine whether loss of cFLIP expression was sufficient to enable LPS-mediated NLRP3 activation, we used cFLIP-tar-

geting small interfering RNA (siRNA) to reduce cFLIP expression. cFLIP knockdown ablated cFLIP expression (Figure S4D), which decreased viability (Figure S4E) and TNF-α secretion (Figure S4F) but did not enable activation of NLRP3 by LPS

alone (Figure S4G). This demonstrates that, while loss of cFLIP is required for NLRP3 activation, it is insufficient to enable it alone.

Butyrate-mediated NLRP3 activation is dependent on caspase-8

The requirement for loss of cFLIP expression suggested that caspase-8 would be required for SCFA-mediated NLRP3 activation. Therefore, we assessed caspase-8 activity in hMDMs following stimulation with LPS, butyrate, or the combination and found that butyrate increased caspase-8 activity in both the absence or presence of LPS (Figure 5A) and that butyrate and propionate, but not nigericin, triggered caspase-8 cleavage (Figure 5B). To determine whether caspase-8 was required for NLRP3 activation, we pre-incubated hMDMs with z-IETD-FMK, a capase-8 inhibitor, prior to stimulation with LPS and butyrate and determined that it inhibited butyrate-mediated NLRP3 activation, as shown by IL-1β release (Figure 5C), IL-1β cleavage (Figure 5D), and caspase-1 cleavage (Figure S5A). IETD substrate cleavage occurred prior to NLRP3 activation, as it was not inhibited by either CP-456,773 or VX-765 (Figure S5B). We confirmed this result by knocking down caspase-8 (Figure S5C), which ablated butyrate-mediated IL-1β release (Figure 5E), IL-1β cleavage (Figure 5F), and caspase-1 cleavage (Figure 5F). In contrast, it had no effect on NLRP3 activation by nigericin (Figure 5F), nor did it alter NLRP3 or pro-IL-1β protein levels (Figure S5C).

Butyrate-mediated NLRP3 activation is restrained by RIPK1-mediated regulation of caspase-8

A key regulator of caspase-8 activation upon inhibition of the NF-κB signaling pathway is receptor-interacting serine/threonine-protein kinase 1 (RIPK1). RIPK1 has both kinase-dependent and -independent functions,[32] and we investigated these using either a RIPK1 inhibitor, Necrostatin-1 (Nec1), or reducing RIPK1 expression with siRNA. Inhibiting RIPK1 kinase activity with Nec1 caused a minor increase in NLRP3 activation by LPS and butyrate (Figure S5D), demonstrating that RIPK1 activity is not required for NLRP3 activation. In contrast, ablating RIPK1 expression using siRNA (Figure 5E) substantially increased IL-1β release (Figure 5G) as well as IL-1β and caspase-1 cleavage (Figure 5H) in response to LPS and butyrate. In contrast, TNF-α was unchanged by both RIPK1 inhibition (Figure S5E) or knockdown (Figure S5F). This was contrary to our expectations, but, under certain circumstances, RIPK1 has been shown to restrict rather than promote caspase-8 activation[33]. Accordingly, we found that RIPK1 knockdown enhanced butyrate-mediated caspase-8 activation (Figure 5I), demonstrating that RIPK1 negatively regulates SCFA-mediated NLRP3 activation by inhibiting caspase-8 activation. Restriction of caspase-8 activity by RIPK1 has been described previously, and in that case, RIPK3 was required for caspase-8 activation (Anderton 2019). Therefore, we investigated whether RIPK3 was required for SCFA-mediated NLRP3 activation by ablating expression with RIPK3 targeting siRNA. However, we were only able to partially ablate RIPK3 expression by siRNA knockdown (Figure S5G), and reduction of RIPK3 to this level had no effect on LPS and butyrate-mediated IL-1β release (Figure S5H).

Loss of IL-10 secretion is required for butyrate-driven NLRP3 inflammasome activation

In addition to causing IL-1β release, butyrate decreased secretion of other cytokines, including IL-6, IL-10, and IL-12p40 (Figure 1A). As our data indicated that loss of cFLIP alone was not sufficient to trigger NLRP3 activation, we hypothesized that further loss of other regulatory mechanisms would be required for NLRP3 activation. IL-10, in particular, is important in maintaining gut homeostasis, and this is partially mediated by inhibition of NLRP3 activation.[34] We first confirmed that butyrate (Figures 6A and S6A) and propionate (Figure S6B) blocked IL-10 secretion. Furthermore, butyrate blocked IL-10 secretion across a range of different TLR ligands (Figure S6C). Similar to *CFLAR* and *XIAP*, the *IL-10* gene locus had little increase in acetylation compared to other expressed genes following butyrate and LPS (Figure 6B). Therefore, we tested whether loss of IL-10 was also due to HDAC inhibition. As we observed with IL-1β release, knocking down single HDACs did not recapitulate the SCFA-driven loss of IL-10 secretion (Figure S4D). However, inhibition of all class 1 HDACs (Figure 6C) was sufficient to inhibit IL-10 secretion. To determine whether loss of IL-10 secretion was a requirement for NLRP3 activation, we treated the cells with LPS and butyrate in the presence or absence of recombinant IL-10. Pre-incubation with IL-10 completely ablated activation of NLRP3 with LPS and butyrate (Figure 6D), demonstrating that loss of IL-10 or other cytokines that activate the same signaling pathways is required for butyrate-mediated NLRP3 activation.

IL-10 has been shown to inhibit NLRP3 through activation of STAT3 in a model of colitis.[21] To determine whether STAT3 was inactivated by pre-treatment with butyrate and LPS, we assessed its phosphorylation at Tyr705, and found that, compared to LPS, phosphorylation was ablated by the addition of butyrate (Figure 6E). This was also observed in response to activation of other TLRs (Figure S6E). Notably, IL-10 rescued STAT3 phosphorylation at Tyr705 (Figure 6E), demonstrating that butyrate inhibits STAT3 activation through inhibition of cytokine transcription. To determine whether loss of IL-10-mediated STAT3 activation was sufficient to activate NLRP3, we blocked the IL-10 receptor or neutralized IL-10 in the presence of LPS. While both treatments increased IL-1β release in the presence of LPS and butyrate (Figures 6F and S6G) neither enabled IL-1β release in the presence of LPS alone (Figures 6F and S6G) or altered TNF-α secretion (Figures S6F and S6G). To confirm this, we ablated STAT3 expression by knockdown (Figure 6G). Similar to inhibition of IL-10, STAT3 knockdown increased IL-1β release in the presence of LPS and butyrate but did not consistently enable IL-1β release by LPS alone, though some donors showed a small increase in IL-1β release (Figure 6G). In contrast, TNF-α secretion was unaltered by STAT3 knockdown (Figure 6H). These results collectively demonstrate that inhibiting IL-10 signaling or STAT3 signaling enhances NLRP3 activation by LPS and butyrate but is insufficient to activate NLRP3.

In other contexts, IL-10 signaling increased expression of cFLIP through STAT3 activation,[35] and so may be inhibiting butyrate-mediated NLRP3 activation by rescuing cFLIP expression. To determine whether this was the case, recombinant IL-10 was added to hMDMs together with LPS in the absence or
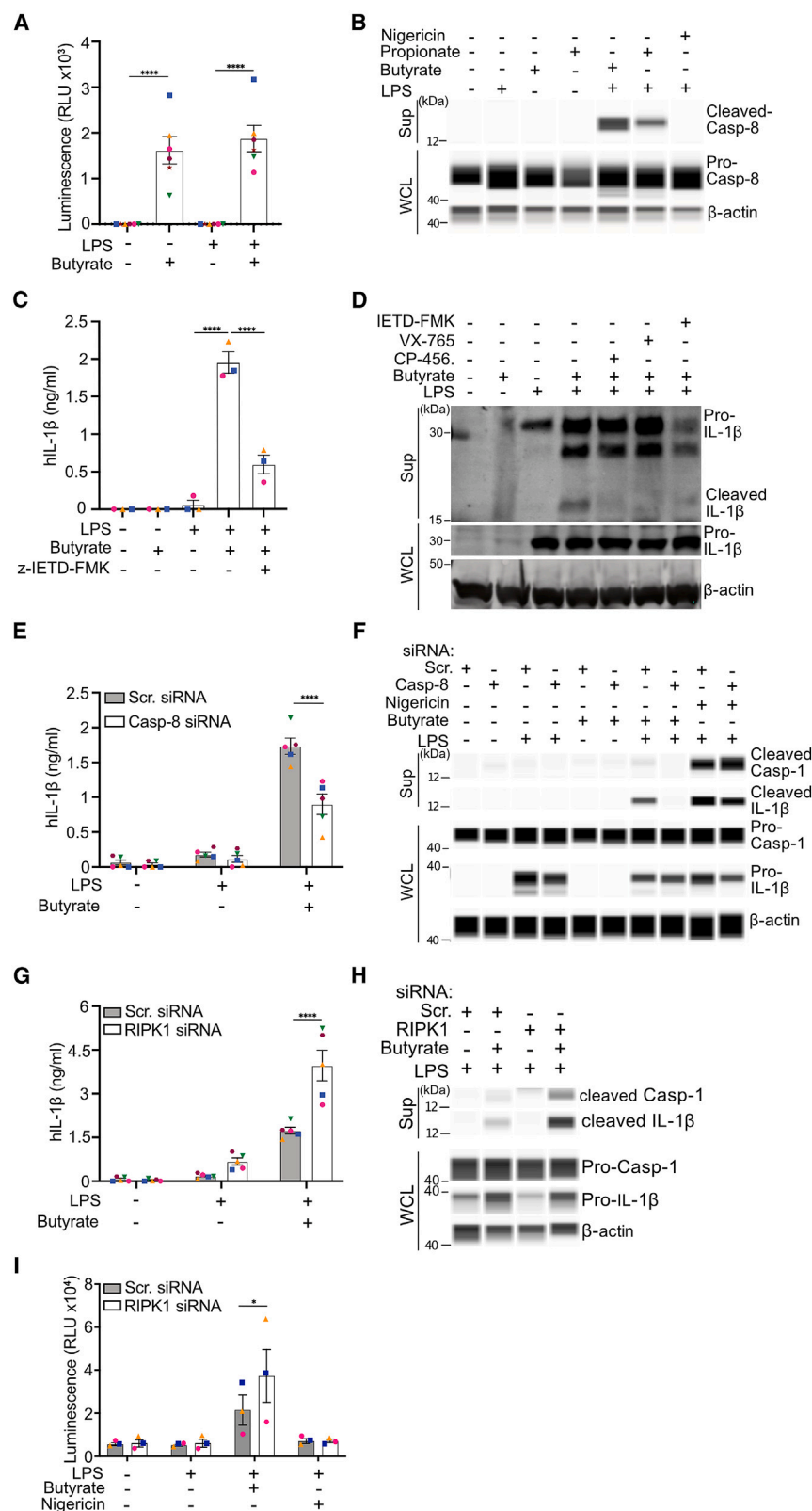
Figure 5. Butyrate-mediated NLRP3 inflammasome activation is dependent on caspase-8 and restrained by RIPK1

(A) hMDMs were incubated with butyrate (10 mM, 16 h) with or without LPS (1 ng/mL, 16 h). Caspase-8 activity was assessed by Caspase-Glo assay; $n = 6$.

(B) hMDMs were treated with LPS (1 ng/mL), butyrate (10 mM), propionate (10 mM), or nigericin (10 μM). Caspase-8 cleavage was assessed by WES; representative of $n = 2$.

(C and D) IL-1β measured from sup (C) and IL-1β assessed from sup or WCL (D). Representative of $n = 3$. hMDMs were treated with LPS (1 ng/mL, 16 h), with or without butyrate (10 mM, 16 h), with or without z-IETD-FMK (5 μM, 30min), or with or without CP-456,773 (2 μM, 30 min) and VX-765 (40 μM, 30 min).

(E and F) IL-1β measured from sup ($n = 5$) (E) and IL-1β and caspase-1 cleavage assessed from sup and WCL (F); representative of $n = 2$. hMDMs were electroporated with either scrambled or caspase-8 siRNA and stimulated with butyrate (10 mM) with or without LPS (1 ng/mL) and with or without nigericin (10 μM).

(G–I) IL-1β from sup $n = 5$ (G) and IL-1β and caspase-1 cleavage assessed from sup and WCL (H); representative of $n = 2$, or caspase-8 activity, $n = 3$ (I). hMDMs were electroporated with either scrambled or RIPK1 siRNA stimulated with butyrate (10 mM) with or without LPS (1 ng/mL) and with or without nigericin (10 μM).

Mean ± SEM are shown; each dot represents one donor. *$p < 0.05$, **$p < 0.01$, ***$p < 0.001$, ****$p < 0.0001$ by either one-way ANOVA with Tukey test (A and C) or two-way ANOVA with Šídák's multiple-comparisons test (E, G, and I).
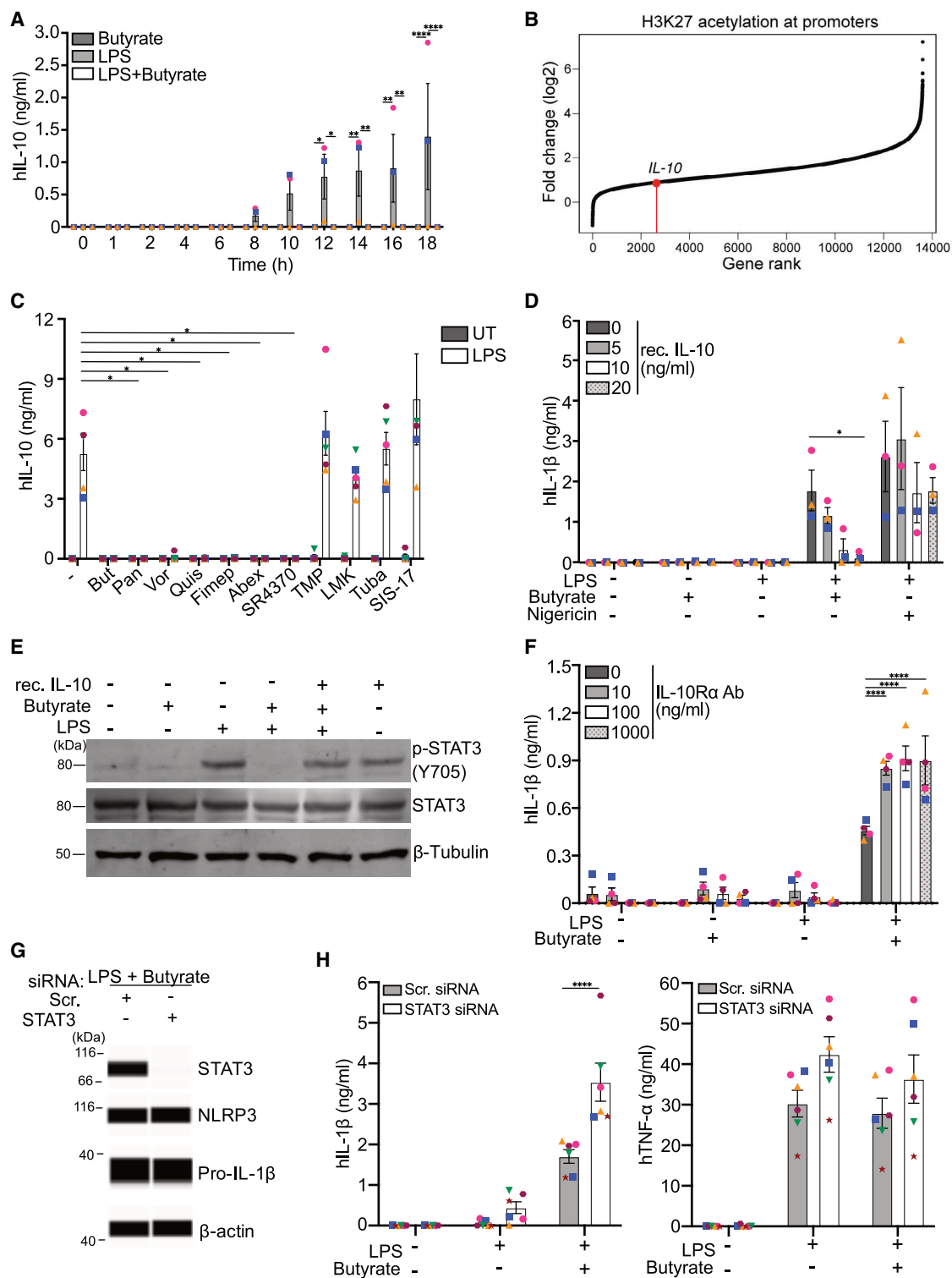
Figure 6. Loss of STAT3-activating cytokines is required for butyrate-driven NLRP3 inflammasome activation

(A) IL-10 measured from sup from hMDMs treated with butyrate (10 mM) with or without LPS (1 ng/mL).

(B) Ranking of all genes ordered by the FC in H3K27ac signal in LPS + butyrate-treated samples.

(C) IL-10 measured from sup from hMDMs treated with LPS with or without HDAC inhibitors.

(legend continued on next page)

presence of butyrate, and the cells were assessed for cFLIP expression. However, IL-10 did not rescue butyrate-mediated expression of either form of cFLIP (Figure S6H), demonstrating that IL-10-mediated inhibition of butyrate-mediated NLRP3 activation is independent of cFLIP regulation.

Butyrate-mediated NLRP3 activation does not trigger cell death but causes gasdermin-D-independent IL-1β secretion

Alongside IL-1β release, NLRP3 activation can also trigger lytic, inflammatory cell death, termed pyroptosis. We assessed pyroptosis in response to LPS and butyrate or propionate but found, surprisingly, that there was no increase in lactate dehydrogenase (LDH) release, a key readout for pyroptosis (Figure 7A). In contrast, nigericin triggered LDH release dependent on both CP-456,773 and VX-765 (Figure S7A). To confirm this, we assessed plasma membrane integrity using an exclusion dye. In contrast to nigericin (Figure 7B), but concordant with the lack of LDH release, LPS and butyrate did not trigger dye uptake or change cell morphology (Figure 7B), suggesting that they do not undergo cell death. As we found no sign of pyroptosis, we assessed cleavage of gasdermin D (gsdmD), the primary effector of pyroptosis, in response to LPS and butyrate. Consistent with our previous results, we did not detect the active p30 C-terminal fragment of gsdmD, which was present in hMDMs treated with LPS and nigericin. Instead, we detected the inactive p43 fragment of gsdmD (Figure 7C).[36] GsdmD knockdown (Figure 7D) demonstrated that gsdmD was not required for LPS and butyrate-mediated IL-1β release (Figure 7E).

The p43 fragment of gsdmD is formed when it is cleaved by caspase-3, which inactivates gsdmD. Therefore, we assessed caspase-3 and caspase-7 cleavage following incubation with LPS and butyrate and found that the active, cleaved forms of both were present in the hMDMs (Figure 7F). Notably, activation of caspase-3 and -7 was independent of pre-incubation with LPS, as observed for butyrate-mediated caspase-8 activation, demonstrating that multiple caspases are activated by butyrate. Gasdermins other than gsdmD have been implicated in both cell death and release of IL-1β, including gasdermin E (gsdmE), which is cleaved and activated by caspase-3.[36] As caspase-3 was also active in these cells, we assessed whether gsdmE was cleaved into its active form but found no difference in cleavage between the LPS condition and either butyrate alone or LPS and butyrate (Figure 7G), indicating that gsdmE is also not required for IL-1β release.

DISCUSSION

SCFAs contribute to both the maintenance of the epithelial barrier and the programming of immune cells under steady-state conditions.[37,38] However, it is unclear what role SCFAs might play in the immune response under conditions where the intestinal barrier has become permeable. Our findings demonstrate that the effects of SCFAs depend on the context in which they are sensed. In contrast to the antimicrobial program engendered by SCFAs on macrophages in steady-state conditions, we show that butyrate and propionate instigate a pro-inflammatory program in the presence of pathogen- and danger-associated molecular patterns. This is primarily mediated through activation of the NLRP3 inflammasome and the subsequent release of IL-1β. NLRP3 could be activated by exposure to butyrate or propionate concurrent with stimulation of any TLR, demonstrating that translocation of any pathogen-derived molecules would be sufficient to trigger IL-1β release in their presence. Concurrently, butyrate and propionate reduced expression and secretion of many LPS-induced cytokines, including the anti-inflammatory molecules IL-10 and IL-1RA, amplifying the effect of NLRP3-dependent IL-1β release. Importantly, butyrate and propionate are produced exclusively by viable bacteria and are sensed by macrophages as danger signals. Therefore, under inflammatory conditions, butyrate and propionate represent viability-associated pathogen-associated molecular patterns (vita-PAMPs), microbially derived products that signal bacterial viability.[39] The requirement for ongoing synthesis of SCFAs is consistent with the two other vita-PAMPS characterized so far, cyclic di-AMP and prokaryotic mRNA, both of which need to be actively synthesized by live bacteria.[40] The action of both butyrate and propionate as danger signals is further evidenced by the inhibition of a key IL-1-regulatory mechanism, IL-1RA, thus ensuring that the IL-1β-mediated pro-inflammatory response is propagated to trigger inflammation.

The vita-PAMP activity of butyrate and propionate is likely to be mediated by their ability to inhibit HDACs. Inhibition of HDACs, specifically HDACs 1–3 and 10, recapitulated both of the effects of butyrate and propionate; namely, activation of NLRP3 and modulation of the LPS-mediated cytokine response. This differentiates them from the two previously described vita-PAMPs, which are detected directly by immune receptors. Notably, HDAC inhibition by either butyrate or TSA caused profound changes in the transcriptome and, in particular, caused the loss of transcription of two important genes required to prevent NLRP3 inflammasome activation, *CFLAR* and *IL10*.

(D) IL-1β measured from sup from hMDMs incubated with LPS (1 ng/mL) and butyrate (10 mM) with or without pre-incubation with recombinant human IL-10 (rhIL-10) (30 min).

(E) hMDMs pre-treated with rhIL-10 (100 ng/mL, 30 min) before treatment with medium, LPS (1 ng/mL, 16 h), and/or butyrate (10 mM, 16 h). Phosphorylated STAT3(Y705), total STAT3, and β-tubulin were measured by immunoblot; representative of *n* = 3.

(F) IL-1β measured from sup from hMDMs pre-incubated with IL-10Rα-blocking antibody for 30 min and subsequent LPS (1 ng/mL, 16 h) and/or butyrate (10 mM, 16 h).

(G) hMDMs electroporated with siRNA targeting STAT3 and incubated with LPS (1 ng/mL, 16 h) with or without butyrate (10 mM, 16 h). STAT3 expression was assayed 3 days post electroporation by WES; representative of *n* = 3.

(H) IL-1β and TNF-α measured from sup.

Mean ± SEM are shown; *n* = 3–6; each dot represents one donor. *$p < 0.05$, **$p < 0.01$, ***$p < 0.001$, ****$p < 0.0001$ by two-way ANOVA with Šídák's multiple-comparisons test.
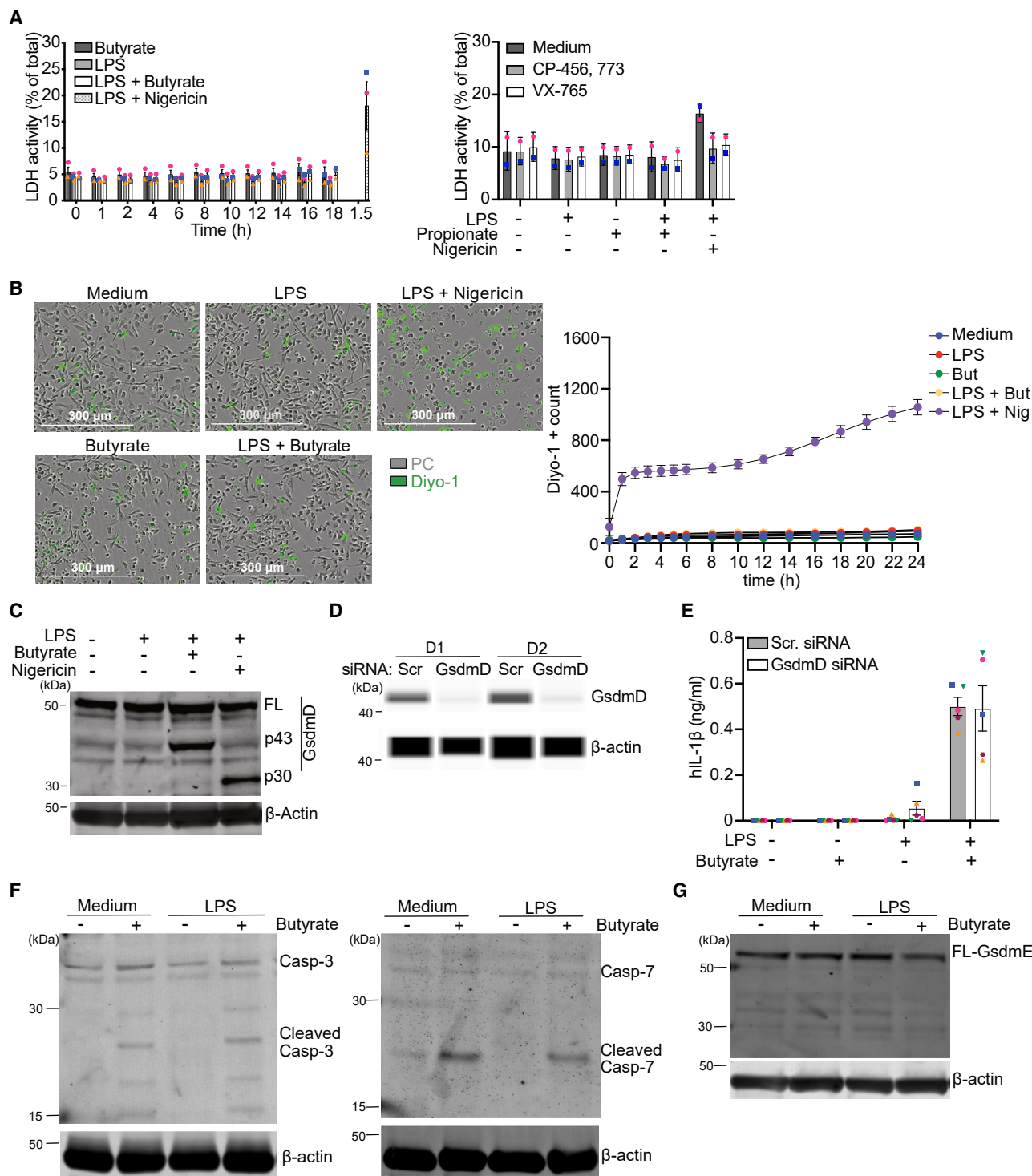
Figure 7. Butyrate-mediated NLRP3 activation triggers IL-1β release independent of gsdmD and cell death

(A) LDH activity measured from sup from hMDMs treated with LPS (1 ng/mL), butyrate (10 mM), or propionate (10 mM), and/or LPS (1 ng/mL, 3 h) with or without nigericin (10 μM, 1.5 h) pre-incubated with or without CP-456,773 (2 μM, 30 min) or VX-765 (40 μM, 30 min).

(B) Fluorescence and bright-field imaging and analysis of hMDMs incubated with LPS (1 ng/mL) with or without butyrate (10 mM) for 24 h or with LPS (10 ng/mL, 3 h) and nigericin (10 μM) in the presence of the viability dye Diyo-1. Shown are representative images from t = 24 h. Quantitation of Diyo-1 positive cells shows mean ± SD, four images/well, used to give average cell count/image/well, representative of *n* = 4.

(legend continued on next page)

Reconstitution or addition of either one of these molecules was sufficient to prevent NLRP3 inflammasome activation, demonstrating that butyrate and propionate engage a multifaceted program to enact NLRP3 inflammasome activation. It was interesting to note that, counterintuitively, loss of *CFLAR* and *IL10* expression occurred despite increasing H3K27ac across the genome. This suggests that HDAC inhibition results in an altered pattern of histone acetylation caused by histone hyperacetylation, which may then overload the transcriptional machinery, resulting in it becoming the limiting factor for transcription. This has been observed previously for interferon-stimulated genes (ISGs), where butyrate and other HDAC inhibitors cause a decrease in ISG expression.[41] This study demonstrated that histone hyperacetylation mediated by HDAC1/2 inhibition resulted in relocalization of Brd4, an epigenetic reader, and the elongation factor P-TEFb, to other histones and away from ISG loci, causing loss of ISG expression. Given the correlation between the loss of expression of cFLIP and XIAP and the lack of increased acetylation, we suggest that expression of these genes may be regulated by the same mechanism. The coupling of expression of ISG and interferon-related genes, which are important for the response to pathogens, to genes essential for the prevention of cell death may be a mechanism to ensure the cell dies if expression of ISGs is interfered with. This is highly relevant to treatment for interferonopathies, where HDAC inhibitors have been proposed as a potential therapy. Further research exploring the link between alteration to histone acetylation and cell death could potentially lead to a better understanding of epigenetic modulation in both pathogen-mediated cell death and HDAC inhibitors as a therapy for auto-inflammatory and immune disorders.

In addition to inhibiting expression of cFLIP, butyrate-mediated NLRP3 activation also required loss of IL-10 expression and secretion. This effect was also likely to be mediated by HDAC inhibition and subsequent loss of transcriptional machinery at the IL-10 locus, as it was also not highly hyperacetylated following treatment with butyrate. IL-10 regulated NLRP3 activation by controlling activation of STAT3, as loss of STAT3 in hMDM resulted in spontaneous NLRP3 activation following incubation with LPS. It was interesting to note here that inhibition of NLRP3 by IL-10 was independent of regulation of cFLIP, implying that the IL-10/STAT3 axis regulates NLRP3 activation independent of caspase-8 activity. This suggests that the presence of IL-10, rather than regulating cell death, will dictate whether caspase-8 dependent cell death is inflammatory, based on whether it activates apoptosis, an immunologically silent form of death, or leads to continued IL-1β release. It also demonstrates that SCFA-driven NLRP3 activation requires multiple, different perturbations of the LPS transcriptome.

The loss of cFLIP expression enabled activation of caspase-8, which was required to subsequently trigger the NLRP3 inflammasome. Caspase-8 activation is a crucial cellular defense mechanism to guard against pathogen-mediated inhibition of the NF-κB-mediated inflammatory response.[42] Indeed, inhibition of TAK1, an essential kinase in the NF-κB signaling pathway, is sufficient to trigger caspase-8-dependent cell death through loss of cFLIP expression.[43] However, beyond inhibition of this signaling cascade, it is unclear how other mechanisms that interfere with expression of inflammatory genes trigger caspase-8 activation. Here we show that epigenetically mediated loss of cFLIP is a new pathway through which this can occur. Further research focusing on pathogen-mediated loss of transcription and translation generally, or specifically for cFLIP, can lead to cell death and promote immunity.

The absence of potassium efflux, ASC speck formation, and cell death accompanying butyrate-mediated NLRP3 activation was surprising. This is reminiscent of the alternative pathway of NLRP3 activation triggered by LPS in monocytes[24] or NLRP3 hyperactivation in response to oxidized PAPC (ox-PAPC),[44] where the cells also release IL-1β without the accompanying cell death. Indeed, despite butyrate-mediated activation of caspase-1, -3, and -7, IL-1β release was independent of gsdmD and gsdmE, consistent with the cells not becoming permeable to the exclusion dye, suggesting that pore-forming proteins are not involved in IL-1β release. It is unclear how IL-1β is released in response to butyrate, though one possibility is the non-classical secretion pathway, which is reliant on the autophagy system and has been shown to release IL-1β in other contexts.[45] Alternatively, it has been shown recently that cleaved IL-1β could be translocated to the Golgi and secreted through the canonical secretion pathway.[46] Further research will be required to delineate the exact mechanism, as well as how the hMDMs survive in spite of having multiple active caspases.

Our results also go some way toward explaining the opposing effects of dietary fiber and SCFAs in IBD, as studies have suggested both beneficial and detrimental effects on the gut health in patients with IBD and in mouse colitis models.[11] They suggest that the timing of the SCFA generation will have an impact on whether they function in an anti- or pro-inflammatory manner. SCFAs that are generated once the intestinal epithelial barrier has been breached and TLR ligands and pro-inflammatory cytokines, including TNF-α, are present and would result in NLRP3 inflammasome activation, thus contributing to the pathogenesis of IBD rather than suppressing it. This would be exacerbated by the SCFA-driven loss of other cytokines, particularly IL-10, and the subsequent absence of STAT3 activation. Further research examining the role of fiber in different stages of IBD will help to elucidate in what contexts they are beneficial and when they may be detrimental.

(C) hMDMs treated with medium, LPS (1 ng/mL), or butyrate (10 mM) for 16 h or LPS (1 ng/mL, 3 h) and nigericin (10 μM, 1.5 h). GsdmD and β-actin were measured from WCL by immunoblot; representative of *n* = 3.
(D) hMDMs electroporated with either scrambled siRNA or gsdmD siRNA. GsdmD and β-actin were measured from WCL by WES.
(E) IL-1β measured from sup from hMDMs treated as in (C).
(F and G) hMDMs treated as in (B) were analyzed for cleaved caspase-3 or cleaved caspase-7 (F) or gsdmE (G) from WCL by immunoblot; all representative of *n* = 2.
Mean ± SEM are shown; n = 3–5; each dot represents one donor.

Limitations of the study

In this study, we demonstrated NLRP3 inflammasome activation in human macrophages upon stimulation with the SCFAs butyrate and propionate. Both butyrate and propionate were used at a concentration of 1–10 mM to stimulate NLRP3 inflammasome activation, but effects at concentrations lower than 1 mM were not examined, with the exception of the effect of SCFAs on IL-10. Therefore, the mechanism we describe will be relevant to sites in the body where these concentrations are generated, including the small and large intestine and the buccal cavity. In contrast, plasma levels of SCFAs in the micromolar range have been reported. Furthermore, due to known differences in NLRP3 inflammasome activation between the human and murine system, the study was conducted with primary human cells isolated from buffy coats, and so the mechanism we describe is relevant to the human system. As a consequence, we did not use murine models of IBD or provide evidence for the *in vivo* role of SCFA sensing and HDAC inhibition. Further studies will be required to prove these pathways in an *in vivo* context.

RESOURCE AVAILABILITY

Lead contact
The lead contact is Eicke Latz (eicke.latz@drfz.de).

Material availability
This study did not generate new unique reagents.

Data and code availability
RNA-seq and ChIP-seq data generated for this study have been deposited at the GEO and are publicly available as of the date of publication under accession number GSE248579.

AUTHOR CONTRIBUTIONS

E.L., M.S.J.M., and B.M. conceived the study. M.S.J.M., W.W., A.D., S.C., and E.L. designed experiments. W.W., A.D., B.M., M.C., K.P., A.W., N.S., T.W., H.F., A.J., R.S., F.D., S.C., and M.S.J.M. performed experiments. L.L., K.P., C.B., S.V.S., and S.C. analyzed and provided the visualization for the RNA-seq and ChIP-seq data. W.W., A.D., B.M., N.S., and M.S.J.M. performed analysis and visualization. M.S.J.M., E.L., S.C., R.C.C., and F.M. supervised the study. M.S.J.M. wrote the manuscript with input from all authors.

STAR★METHODS

Detailed methods are provided in the online version of this paper and include the following:

- KEY RESOURCES TABLE
- EXPERIMENTAL MODEL AND SUBJECT DETAILS
- METHOD DETAILS
  - Isolation and culturing of primary human macrophages
  - Inflammasome stimulation
  - Measurement of cytokine secretion
  - Caspase-8 activity assay
  - Lactate dehydrogenase (LDH) assay
  - Small interfering RNA (siRNA) electroporation in primary human macrophages
  - Cloning
  - Lentiviral transduction of primary human macrophages
  - Cellular potassium quantification
  - Immunoblotting
  - Simple Western assay on WesTM
  - Live cell imaging for cell death analysis
  - ASC speck imaging and quantitation
  - Gene expression analysis by quantitative PCR (qPCR)
  - RNA-sequencing
  - RNA-sequencing analysis
  - ChIP-seq
  - ChIP-seq data processing
  - GSEA
  - Motif enrichment
  - Mass spectrometry-based proteomics (MS)
  - MS data processing and analysis
- QUANTIFICATION AND STATISTICAL ANALYSIS

SUPPLEMENTAL INFORMATION

Supplemental information can be found online at https://doi.org/10.1016/j.celrep.2024.114736.

REFERENCES

1. van der Hee, B., and Wells, J.M. (2021). Microbial Regulation of Host Physiology by Short-chain Fatty Acids. Trends Microbiol. *29*, 700–712. https://doi.org/10.1016/j.tim.2021.02.001.

2. Magrin, G.L., Strauss, F.J., Benfatti, C.A.M., Maia, L.C., and Gruber, R. (2020). Effects of Short-Chain Fatty Acids on Human Oral Epithelial Cells and the Potential Impact on Periodontal Disease: A Systematic Review of In Vitro Studies. Int. J. Mol. Sci. *21*, 4895. https://doi.org/10.3390/ijms21144895.

3. Priyadarshini, M., Kotlo, K.U., Dudeja, P.K., and Layden, B.T. (2018). Role of Short Chain Fatty Acid Receptors in Intestinal Physiology and Pathophysiology. Compr. Physiol. *8*, 1091–1115. https://doi.org/10.1002/cphy.c170050.

4. Waldecker, M., Kautenburger, T., Daumann, H., Busch, C., and Schrenk, D. (2008). Inhibition of histone-deacetylase activity by short-chain fatty

acids and some polyphenol metabolites formed in the colon. J. Nutr. Biochem. 19, 587–593.

5. Donohoe, D.R., Garge, N., Zhang, X., Sun, W., O'Connell, T.M., Bunger, M.K., and Bultman, S.J. (2011). The Microbiome and Butyrate Regulate Energy Metabolism and Autophagy in the Mammalian Colon. Cell Metabol. 13, 517–526. https://doi.org/10.1016/j.cmet.2011.02.018.

6. Schulthess, J., Pandey, S., Capitani, M., Rue-Albrecht, K.C., Arnold, I., Franchini, F., Chomka, A., Ilott, N.E., Johnston, D.G.W., Pires, E., et al. (2019). The Short Chain Fatty Acid Butyrate Imprints an Antimicrobial Program in Macrophages. Immunity 50, 432–445.e7. https://doi.org/10.1016/j.immuni.2018.12.018.

7. Lee, S.H., Kwon, J.E., and Cho, M.-L. (2018). Immunological pathogenesis of inflammatory bowel disease. Int. Res. 16, 26–42. https://doi.org/10.5217/ir.2018.16.1.26.

8. Gearry, R.B., Irving, P.M., Barrett, J.S., Nathan, D.M., Shepherd, S.J., and Gibson, P.R. (2009). Reduction of dietary poorly absorbed short-chain carbohydrates (FODMAPs) improves abdominal symptoms in patients with inflammatory bowel disease—a pilot study. J. Crohn's Colitis 3, 8–14. https://doi.org/10.1016/j.crohns.2008.09.004.

9. Maagaard, L., Ankersen, D.V., Végh, Z., Burisch, J., Jensen, L., Pedersen, N., and Munkholm, P. (2016). Follow-up of patients with functional bowel symptoms treated with a low FODMAP diet. World J. Gastroenterol. 22, 4009–4019. https://doi.org/10.3748/wjg.v22.i15.4009.

10. Armstrong, H.K., Bording-Jorgensen, M., Santer, D.M., Zhang, Z., Valcheva, R., Rieger, A.M., Sung-Ho Kim, J., Dijk, S.I., Mahmood, R., Ogungbola, O., et al. (2023). Unfermented β-fructan Fibers Fuel Inflammation in Select Inflammatory Bowel Disease Patients. Gastroenterology 164, 228–240. https://doi.org/10.1053/j.gastro.2022.09.034.

11. Singh, V., Yeoh, B.S., Walker, R.E., Xiao, X., Saha, P., Golonka, R.M., Cai, J., Bretin, A.C.A., Cheng, X., Liu, Q., et al. (2019). Microbiota fermentation-NLRP3 axis shapes the impact of dietary fibres on intestinal inflammation. Gut 68, 1801–1812. https://doi.org/10.1136/gutjnl-2018-316250.

12. Hartman, D.S., Tracey, D.E., Lemos, B.R., Erlich, E.C., Burton, R.E., Keane, D.M., Patel, R., Kim, S., Bhol, K.C., Harris, M.S., and Fox, B.S. (2016). Effects of AVX-470, an Oral, Locally Acting Anti-Tumour Necrosis Factor Antibody, on Tissue Biomarkers in Patients with Active Ulcerative Colitis. J. Crohn's Colitis 10, 641–649. https://doi.org/10.1093/ecco-jcc/jjw026.

13. Danese, S., Vermeire, S., Hellstern, P., Panaccione, R., Rogler, G., Fraser, G., Kohn, A., Desreumaux, P., Leong, R.W., Comer, G.M., et al. (2019). Randomised trial and open-label extension study of an anti-interleukin-6 antibody in Crohn's disease (ANDANTE I and II). Gut 68, 40–48. https://doi.org/10.1136/gutjnl-2017-314562.

14. Simon, E.G., Ghosh, S., Iacucci, M., and Moran, G.W. (2016). Ustekinumab for the treatment of Crohn's disease: can it find its niche? Therap. Adv. Gastroenterol. 9, 26–36. https://doi.org/10.1177/1756283x15618130.

15. Hanaei, S., Sadr, M., Rezaei, A., Shahkarami, S., Daryani, N.E., Bidoki, A.Z., and Rezaei, N. (2018). Association of NLRP3 single nucleotide polymorphisms with ulcerative colitis: A case-control study. Clin. Res. Hepatol. Gastroenterol. 42, 269–275. https://doi.org/10.1016/j.clinre.2017.09.003.

16. Villani, A.-C., Lemire, M., Fortin, G., Louis, E., Silverberg, M.S., Collette, C., Baba, N., Libioulle, C., Belaiche, J., Bitton, A., et al. (2009). Common variants in the NLRP3 region contribute to Crohn's disease susceptibility. Nat. Genet. 41, 71–76. https://doi.org/10.1038/ng.285.

17. Perera, A.P., Fernando, R., Shinde, T., Gundamaraju, R., Southam, B., Sohal, S.S., Robertson, A.A.B., Schroder, K., Kunde, D., and Eri, R. (2018). MCC950, a specific small molecule inhibitor of NLRP3 inflammasome attenuates colonic inflammation in spontaneous colitis mice. Sci. Rep. 8, 8618. https://doi.org/10.1038/s41598-018-26775-w.

18. Hirota, S.A., Ng, J., Lueng, A., Khajah, M., Parhar, K., Li, Y., Lam, V., Potentier, M.S., Ng, K., Bawa, M., et al. (2011). NLRP3 inflammasome plays a key role in the regulation of intestinal homeostasis. Inflamm. Bowel Dis. 17, 1359–1372. https://doi.org/10.1002/ibd.21478.

19. Bauer, C., Duewell, P., Lehr, H.-A., Endres, S., and Schnurr, M. (2012). Protective and Aggravating Effects of Nlrp3 Inflammasome Activation in IBD Models: Influence of Genetic and Environmental Factors. Dig. Dis. 30, 82–90. https://doi.org/10.1159/000341681.

20. Zaki, M.H., Boyd, K.L., Vogel, P., Kastan, M.B., Lamkanfi, M., and Kanneganti, T.-D. (2010). The NLRP3 Inflammasome Protects against Loss of Epithelial Integrity and Mortality during Experimental Colitis. Immunity 32, 379–391. https://doi.org/10.1016/j.immuni.2010.03.003.

21. Ip, W.K.E., Hoshi, N., Shouval, D.S., Snapper, S., and Medzhitov, R. (2017). Anti-inflammatory effect of IL-10 mediated by metabolic reprogramming of macrophages. Science 356, 513–519. https://doi.org/10.1126/science.aal3535.

22. Gaidt, M.M., Ebert, T.S., Chauhan, D., Schmidt, T., Schmid-Burgk, J.L., Rapino, F., Robertson, A.A.B., Cooper, M.A., Graf, T., and Hornung, V. (2016). Human Monocytes Engage an Alternative Inflammasome Pathway. Immunity 44, 833–846. https://doi.org/10.1016/j.immuni.2016.01.012.

23. Mangan, M.S.J., Olhava, E.J., Roush, W.R., Seidel, H.M., Glick, G.D., and Latz, E. (2018). Targeting the NLRP3 inflammasome in inflammatory diseases. Nat. Rev. Drug Discov. 17, 588–606. https://doi.org/10.1038/nrd.2018.97.

24. Gaidt, M.M., Ebert, T.S., Chauhan, D., Schmidt, T., Schmid-Burgk, J.L., Rapino, F., Robertson, A.A.B., Cooper, M.A., Graf, T., and Hornung, V. (2016). Human Monocytes Engage an Alternative Inflammasome Pathway. Immunity 44, 833–846. https://doi.org/10.1016/j.immuni.2016.01.012.

25. Kiefer, J., Beyer-Sehlmeyer, G., and Pool-Zobel, B.L. (2006). Mixtures of SCFA, composed according to physiologically available concentrations in the gut lumen, modulate histone acetylation in human HT29 colon cancer cells. Br. J. Nutr. 96, 803–810. https://doi.org/10.1017/bjn20061948.

26. Waldecker, M., Kautenburger, T., Daumann, H., Busch, C., and Schrenk, D. (2008). Inhibition of histone-deacetylase activity by short-chain fatty acids and some polyphenol metabolites formed in the colon. J. Nutr. Biochem. 19, 587–593. https://doi.org/10.1016/j.jnutbio.2007.08.002.

27. Park, S.-Y., and Kim, J.-S. (2020). A short guide to histone deacetylases including recent progress on class II enzymes. Exp. Mol. Med. 52, 204–212. https://doi.org/10.1038/s12276-020-0382-4.

28. Jorgensen, I., Rayamajhi, M., and Miao, E.A. (2017). Programmed cell death as a defence against infection. Nat. Rev. Immunol. 17, 151–164. https://doi.org/10.1038/nri.2016.147.

29. Lawlor, K.E., Feltham, R., Yabal, M., Conos, S.A., Chen, K.W., Ziehe, S., Graß, C., Zhan, Y., Nguyen, T.A., Hall, C., et al. (2017). XIAP Loss Triggers RIPK3- and Caspase-8-Driven IL-1β Activation and Cell Death as a Consequence of TLR-MyD88-Induced cIAP1-TRAF2 Degradation. Cell Rep. 20, 668–682. https://doi.org/10.1016/j.celrep.2017.06.073.

30. Vince, J.E., Wong, W.W.-L., Gentle, I., Lawlor, K.E., Allam, R., O'Reilly, L., Mason, K., Gross, O., Ma, S., Guarda, G., et al. (2012). Inhibitor of Apoptosis Proteins Limit RIP3 Kinase-Dependent Interleukin-1 Activation. Immunity 36, 215–227. https://doi.org/10.1016/j.immuni.2012.01.012.

31. Golks, A., Brenner, D., Fritsch, C., Krammer, P.H., and Lavrik, I.N. (2005). c-FLIPR, a New Regulator of Death Receptor-induced Apoptosis. J. Biol. Chem. 280, 14507–14513. https://doi.org/10.1074/jbc.m414425200.

32. Vangelis, K., Snehlata, K., Katerina, V., and Manolis, P. (2017). The interplay of IKK, NF-κB and RIPK1 signaling in the regulation of cell death, tissue homeostasis and inflammation. Immunol. Rev. 277, 113–127. https://doi.org/10.1111/imr.12550.

33. Anderton, H., Bandala-Sanchez, E., Simpson, D.S., Rickard, J.A., Ng, A.P., Rago, L.D., Hall, C., Vince, J.E., Silke, J., Liccardi, G., et al. (2019). RIPK1 prevents TRADD-driven, but TNFR1 independent, apoptosis during development. Cell Death Differ. 26, 877–889. https://doi.org/10.1038/s41418-018-0166-8.

34. Gurung, P., Li, B., Subbarao Malireddi, R.K., Lamkanfi, M., Geiger, T.L., and Kanneganti, T.-D. (2015). Chronic TLR Stimulation Controls NLRP3 Inflammasome Activation through IL-10 Mediated Regulation of NLRP3

Expression and Caspase-8 Activation. Sci. Rep. *5*, 14488. https://doi.org/10.1038/srep14488.

35. Du, J., Wu, J., Fu, X., Tse, A.K.-W., Li, T., Su, T., and Yu, Z.-L. (2016). Icariside II overcomes TRAIL resistance of melanoma cells through ROS-mediated downregulation of STAT3/cFLIP signaling. Oncotarget *7*, 52218–52229. https://doi.org/10.18632/oncotarget.10582.

36. Liu, X., Xia, S., Zhang, Z., Wu, H., and Lieberman, J. (2021). Channelling inflammation: gasdermins in physiology and disease. Nat. Rev. Drug Discov. *20*, 384–405. https://doi.org/10.1038/s41573-021-00154-z.

37. Schulthess, J., Pandey, S., Capitani, M., Rue-Albrecht, K.C., Arnold, I., Franchini, F., Chomka, A., Ilott, N.E., Johnston, D.G.W., Pires, E., et al. (2019). The Short Chain Fatty Acid Butyrate Imprints an Antimicrobial Program in Macrophages. Immunity *50*, 432–445.e7. https://doi.org/10.1016/j.immuni.2018.12.018.

38. Donohoe, D.R., Garge, N., Zhang, X., Sun, W., O'Connell, T.M., Bunger, M.K., and Bultman, S.J. (2011). The Microbiome and Butyrate Regulate Energy Metabolism and Autophagy in the Mammalian Colon. Cell Metabol. *13*, 517–526. https://doi.org/10.1016/j.cmet.2011.02.018.

39. Mourao-Sa, D., Roy, S., and Blander, J.M. (2013). Crossroads Between Innate and Adaptive Immunity IV. Adv. Exp. Med. Biol. *785*, 1–8. https://doi.org/10.1007/978-1-4614-6217-0_1.

40. Blander, J.M., and Barbet, G. (2018). Exploiting vita-PAMPs in vaccines. Curr. Opin. Pharmacol. *41*, 128–136. https://doi.org/10.1016/j.coph.2018.05.012.

41. Marié, I.J., Chang, H.-M., and Levy, D.E. (2018). HDAC stimulates gene expression through BRD4 availability in response to IFN and in interferonopathies. J. Exp. Med. *215*, 3194–3212. https://doi.org/10.1084/jem.20180520.

42. Jorgensen, I., Rayamajhi, M., and Miao, E.A. (2017). Programmed cell death as a defence against infection. Nat. Rev. Immunol. *17*, 151–164. https://doi.org/10.1038/nri.2016.147.

43. Muendlein, H.I., Jetton, D., Connolly, W.M., Eidell, K.P., Magri, Z., Smirnova, I., and Poltorak, A. (2020). cFLIPL protects macrophages from LPS-induced pyroptosis via inhibition of complex II formation. Science *367*, 1379–1384. https://doi.org/10.1126/science.aay3878.

44. Zanoni, I., Tan, Y., Di Gioia, M., Springstead, J.R., and Kagan, J.C. (2017). By Capturing Inflammatory Lipids Released from Dying Cells, the Receptor CD14 Induces Inflammasome-Dependent Phagocyte Hyperactivation. Immunity *47*, 697–709.e3. https://doi.org/10.1016/j.immuni.2017.09.010.

45. Claude-Taupin, A., Bissa, B., Jia, J., Gu, Y., and Deretic, V. (2018). Role of autophagy in IL-1β export and release from cells. Semin. Cell Dev. Biol. *83*, 36–41. https://doi.org/10.1016/j.semcdb.2018.03.012.

46. Caielli, S., Balasubramanian, P., Rodriguez-Alcazar, J., Balaji, U., Wan, Z., Baisch, J., Smitherman, C., Walters, L., Sparagana, P., Nehar-Belaid, D., et al. (2023). An unconventional mechanism of IL-1β secretion that requires Type I IFN in lupus monocytes. Preprint at bioRxiv. https://doi.org/10.1101/2023.08.03.551696.

47. Bobadilla, S., Sunseri, N., and Landau, N.R. (2013). Efficient transduction of myeloid cells by an HIV-1-derived lentiviral vector that packages the Vpx accessory protein. Gene Ther. *20*, 514–520. https://doi.org/10.1038/gt.2012.61.

48. Love, M.I., Huber, W., and Anders, S. (2014). Moderated estimation of fold change and dispersion for RNA-seq data with DESeq2. Genome Biol. *15*, 550. https://doi.org/10.1186/s13059-014-0550-8.

49. Langmead, B., and Salzberg, S.L. (2012). Fast gapped-read alignment with Bowtie 2. Nat. Methods *9*, 357–359. https://doi.org/10.1038/nmeth.1923.

50. Zhang, Y., Liu, T., Meyer, C.A., Eeckhoute, J., Johnson, D.S., Bernstein, B.E., Nusbaum, C., Myers, R.M., Brown, M., Li, W., and Liu, X.S. (2008). Model-based Analysis of ChIP-Seq (MACS). Genome Biol. *9*, R137. https://doi.org/10.1186/gb-2008-9-9-r137.

51. Subramanian, A., Tamayo, P., Mootha, V.K., Mukherjee, S., Ebert, B.L., Gillette, M.A., Paulovich, A., Pomeroy, S.L., Golub, T.R., Lander, E.S., and Mesirov, J.P. (2005). Gene set enrichment analysis: A knowledge-based approach for interpreting genome-wide expression profiles. Proc. Natl. Acad. Sci. USA *102*, 15545–15550. https://doi.org/10.1073/pnas.0506580102.

52. Heinz, S., Benner, C., Spann, N., Bertolino, E., Lin, Y.C., Laslo, P., Cheng, J.X., Murre, C., Singh, H., and Glass, C.K. (2010). Simple Combinations of Lineage-Determining Transcription Factors Prime cis-Regulatory Elements Required for Macrophage and B Cell Identities. Mol. Cell *38*, 576–589. https://doi.org/10.1016/j.molcel.2010.05.004.

STAR★METHODS

KEY RESOURCES TABLE

REAGENT or RESOURCE	SOURCE	IDENTIFIER
Antibodies		
beta-Actin	Licor	926–42212
beta-Tubulin	Cell Signaling Technology	2128S
NLRP3 (D4D8T)	Cell Signaling Technology	15101S
IL-1beta	R&D systems	BAF201
XIAP	Cell Signaling Technology	2042
cFLIP (D5J1E)	Cell Signaling Technology	56343
Pro-IL-1β	abcam	Ab2105
Cleaved Caspase-1 (ASP297)	Cell Signaling Technology	4199
Caspase-8	Cell Signaling Technology	9746
RIPK1	Cell Signaling Technology	D94C12
cleaved Caspase-3 (Asp175)	Cell Signaling Technology	9664
cleaved caspase-7(Asp198)	Cell Signaling Technology	9491
HDAC1	Pierce	PA1-860
HDAC2	Cell Signaling Technology	2540S
HDAC3	Cell Signaling Technology	85057S
STAT3	Cell Signaling Technology	9132
p-STAT3	Cell Signaling Technology	9145
Gasdermin D	Sigma (Atlas)	HPA044487
DFNA5/GSDME	Abcam	ab215191
Histone 3	Cell Signaling Technology	9715S
H3K27Ac	Cell Signaling Technology	8173
H3K27Ac	Abcam	ab4729
NFkB (p65)	Cell Signaling Technology	6956
pNFkB (p65)	Cell Signaling Technology	4764S
IL-10 Neutralisation Antibody	R&D Systems	MAB217
Anti-rabbit IRDye 680RD	Li-Cor	926–68073
ASC	Biolegend	HASC-71
Anti-mouse IRDye 800CW	Li-Cor	926–32212
Anti-mouse IRDye 680RD	Li-Cor	926–68072
Anti-rabbit IRDye 800CW	Li-Cor	926–32213
Anti-rabbit IRDye 680RD	Li-Cor	926–68073
Bacterial and virus strains		
DH5α	LifeTechnologies	18265017
DH10α	ThermoFischer	EC0113
Biological samples		
Buffy coat	Unikliniken Bonn Blood donation center	N/A
Chemicals, peptides, and recombinant proteins		
DMEM Medium	Thermo Fisher	12634010
RPMI 1640 Medium	Thermo Fisher	21875–091
DPBS	Thermo Fisher	14190–169
FCS	Thermo Fisher	10270106/3475027 S2
PenStrep	Lifetechnologies	15140–122
Ficoll–Paque PLUS	GE Healthcare	17-1440-03
CD14 MicroBeads UltraPure (human)	Miltenyi Biotech	130-118-906

Continued

REAGENT or RESOURCE	SOURCE	IDENTIFIER
rhGM-CSF	ImmunoTools	11343125
GlutaMAX	Thermo Fisher	35050–038
Sodium pyruvate	Thermo Fisher	11360039
LPS ultrapure EB	Invivogen	tlrl-smlps
Sodium butyrate	Sigma	303410
cOmplete EDTA-free Protease Inhibitor Cocktail Tablet	Roche	4693132001
PhosStop Easypack Phosphatase Inhibitor Cocktail Tablets	Sigma-Aldrich	4906837001
Tris-HCl	Sigma	T2694-100mL
NaCl	VWR	1.06404.5000
EDTA	Sigma	03690-100mL
Triton X-100	Carl Roth	3051,3
Glycerol	Merck	8.18709.1000
SDS	Sigma	L4509
Deoxycholate	Sigma	30970-100G
NuPAGE LDS sample Buffer (4x)	Invitrogen	NP0008
Pierce^{TM} DTT (Dithiothreitol), No-Weigh^{TM} Format	Thermo Fisher	A39255
PageRuler Plus Prestained Protein Ladder	ThermoScientific	26619
NuPAGE Mops SDS running buffer 20x	Invitrogen	NP0001-02
NuPAGE Mes SDS running buffer 20x	Invitrogen	NP0002-02
Anti-Rabbit Detection Module for Jess/Wes	Biotechne	DM-001
Anti-Mouse Detection Module for Jess/Wes	Biotechne	DM-002
Anti-Goat Detection Module for Jess/Wes	Biotechne	DM-006
Nigericin (Sodium salt), 10mg	Cayman Chemical	Cay11437-10
Emricasan	Sigma/Merck	SML2227-25MG
Necrostatin-1	Tocris	2324
CP-456	Tocris	5479/10
16% Formaldehyde (w/v), Methanol-free	ThermoFisher	28908
FcR Blocking Reagent, human	Milltenyi	130-059-901
CytoVista^{TM} Permeabilization Buffer	Thermo Fisher	V11313
Hoechst 34580	Thermo Fisher	H21486
Sodium Acetate	Sigma	S6636-250G
Sodium Propionate	Sigma	P5436-100G
TSA in DMSO (Trichostatin A)	Merck	T1952
Trizol	Thermo Fisher	15596018
RNeasy Mini Kit	Qiagen	74104
TruSeq RNA Sample Preparation Kit v2	Illumina	RS-122-2001
SPRIBeads	Beckman-Coulter	A47942
KAPA Library Quantification Kits	Kapa Biosystems	07960140001
Acetone (HPLC) Fischer	Thermo Fisher	10417440
Sodium Deoxycholate ≥97% 100g (SDC)	Merck	D6750-100G
5 mL - Bond-Breaker^{TM} TCEP Solution, Neutral pH	Thermo Fisher	77720
BCA Protein Assay Kit	Thermo Fisher	23227
Trypsin/Lys-C Mix, Mass Spec Grade	Promega	V5072
CDS Empore^{TM} SDB-RPS Extraction Disks, 4.7 cm diameter	affinisep	SPE-Disks-Bio-RPS-*M*-47.20
Pierce Acetonitrile (ACN)	Thermo Fisher	TS-51101
Pierce^{TM} Trifluoressigsäure (TFA)	Thermo Fisher	85183
ReproSil-Pur 120 C18-AQ, 1.9 μm beads	Dr. Maisch	r119.b9.
Formic Acid (FA)	Sigma	5330020050
Human IL1 beta HTRF kit	Cisbio	62HIL1BPEH

Continued

REAGENT or RESOURCE	SOURCE	IDENTIFIER
Human IL10 HTRF kit	Cisbio	6FH10PEB
Human TNF alpha HTRF kit	Cisbio	62HTNFAPEH
Human Monocyte Isolation kit	Stemcell	19059
CyQUANT LDH cytotoxicity assay kit	Thermo Fisher	C20301
VX-765	Selleckchem	S2228
Pam3CSK4	Invitrogen	tlrl-pms
Flagellin	Invitrogen	tlrl-bsfla
R848	Invitrogen	tlrl-r848-5
Panobinostat (LBH589)	Biomol	B2764-Cay13280-5
SR-4370	Biomol	Cay25543-1
Abexinostat (PCI-24781)	Biomol	Cay20059-1
TMP195	Biomol	Cay23242-1
Fimepinostat (CUDC-907)	Biomol	Cay25651-5
Quisinostat (JNJ-26481585)	Biomol	B2764-Cay14088-1
Vorinostat (SAHA)	Biomol	SML0061
Tubacin	Biomol	SML0065
LMK-235	Biomol	SML1053
SIS17	Biomol	B7235-A18463-5
Z-IETD-FMK	R&D Systems	FMK007
rhIL-10	Immunotools	11340105
rhIL-6	Immunotools	11340066
Bortezomib PS-341	Selleckchem	S1013
PureLink HiPure Plasmid Filter Maxiprep Kit	Thermo Fisher	K210017
PureLink™ Quick Gel Extraction Kit-50	Thermo Fisher	K210012
PureLink Quick Plasmid Miniprep Kit (250)	Thermo Fisher	K210011
FastDigest NotI	Thermo Fisher	FD0596
FastDigest® AscI (SgsI)	Thermo Fisher	FD1894
Fast SYBR Green Master Mix	Applied Biosystems	4385612
Oligo (dT)18 primer	Thermo Fisher	S0132
dNTPs	Thermo Fisher	R0192
Diyo-1	VWR	76482–918
DRAQ-7	Thermo Fisher	D15106
SuperScript III Reverse Transcriptase	Thermo Fisher	18080–044
Protein G Dynabeads	Invitrogen	10003D
Proteinase K	Qiagen	1014023
ChIP DNA Clean & Concentrator Kit	Zymo	D5205
NEBNext Ultra DNA Library Prep kit	New England Labs	E7645
Experimental models: Cell lines		
HEK-293T cells	ATCC	CRL-3216™
Deposited data		
RNA-seq and ChIP-seq data from Figure 3	Gene Expression Omnibus	GSE248579
Consumables		
μ-slide 8 well ibi-treat, tissue culture treated, sterile	Ibidi	80826
NuPAGE Novex 4–12% Bis-Tris Gels (1.0-mm thick, 15-well)	Invitrogen	NP0323BOX
NuPAGE Novex 10% Bis-Tris Protein Gels, 1.5 mm, 10 well	Invitrogen	NP0315BOX
6-well Nunclon delta surface	Thermo Fisher	140685
12-well tissue culture plate	Sarstedt	83.3921
24-well tissue culture plate	Sarstedt	83.3922
96-well tissue culture plate	Thermo Fisher	08-772-3

(Continued on next page)

Continued

REAGENT or RESOURCE	SOURCE	IDENTIFIER
384-well F-bottom plate, white	Labomedic	784075
Nunc 384-Well Clear Polystyrene Plates with Nontreated Surface	Thermo Fisher	262160
Oligonucleotides		
Silencer ™ Select Negative Control No. 1 siRNA	Thermo Fisher	4390843
Silencer ™ Select siRNA NLRP3 human s41554	Thermo Fisher	4392420
Silencer ™ Select siRNA NLRP3 human s41556	Thermo Fisher	4392420
Silencer ™ Select siRNA HDAC1 human s73	Thermo Fisher	4390824
Silencer ™ Select siRNA HDAC1 human s74	Thermo Fisher	4392420
Silencer ™ Select siRNA HDAC2 human s6495	Thermo Fisher	4390824
Silencer ™ Select siRNA HDAC2 human s6493	Thermo Fisher	4390824
Silencer ™ Select siRNA HDAC3 human s16876	Thermo Fisher	4390824
Silencer ™ Select siRNA HDAC3 human s16877	Thermo Fisher	4390824
Silencer ™ Select siRNA HDAC4 human s18839	Thermo Fisher	4392420
Silencer ™ Select siRNA HDAC4 human s18839	Thermo Fisher	4392420
Silencer ™ Select siRNA HDAC5 human s19462	Thermo Fisher	4390824
Silencer ™ Select siRNA HDAC5 human s19463	Thermo Fisher	4390824
Silencer ™ Select siRNA HDAC6 human s19459	Thermo Fisher	4392420
Silencer ™ Select siRNA HDAC6 human s19461	Thermo Fisher	4392420
Silencer ™ Select siRNA HDAC7 human s28336	Thermo Fisher	4392420
Silencer ™ Select siRNA HDAC7 human s28335	Thermo Fisher	4392420
Silencer ™ Select siRNA HDAC8 human s31698	Thermo Fisher	4390824
Silencer ™ Select siRNA HDAC8 human s31697	Thermo Fisher	4390824
Silencer ™ Select siRNA RIPK3 human s21740	Thermo Fisher	4392420
Silencer ™ Select siRNA RIPK3 human s21742	Thermo Fisher	4392420
Silencer ™ Select siRNA CFLAR human s229912	Thermo Fisher	4392420
Silencer ™ Select siRNA CFLAR human s16864	Thermo Fisher	4392420
Silencer ™ Select siRNA Caspase-8 human s2426	Thermo Fisher	4390824
Silencer ™ Select siRNA Caspase-8 human s2427	Thermo Fisher	4390824
Silencer ™ Select siRNA Gasdermin D human s36339	Thermo Fisher	4392420
qPCR Primer hHPRT-Fw: TCAGGCAGTATAATCCAAAGATGGT	Metabion	N/A
qPCR Primer hHPRT-Rv: AGTCTGGCTTATATCCAACACTTCG	Metabion	N/A
qPCR Primer hZBP-1-Fw: AACATGCAGCTACAATTCCAGA	Metabion	N/A
qPCR Primer hZBP-1-Rv: AGTCTCGGTTCACATCTTTTGC	Metabion	N/A
AscI-frame T-Kozak-CFlar fwd: GGCGCGCCTG CCACCATGTCTGCTGAAGTCATCCATC	Metabion	N/A
NotI-CFlar rev: GCGGCCGCTGTGTAGG AGAGGATAAGTTTCTTTC	Metabion	N/A
Recombinant DNA		
psPAX2-Gag-Pol CMV Enhancer-Chicken Beta Actin-GagPol-RRE-Rabbit Globulin Terminator	–	N/A
pMD2.G CMV Enhancer-CMV-VSVG-Human beta Globulin Terminator	–	N/A
pInducer20 minus mPGK-hCflar wt v5-T2A-mCherry-hPGK-Puromycin	CFLAR insert from Addgene	#82936
pInducer20 minus mPGK-MCS-T2A-mCherry-hPGK-Puromycin	–	N/A

(Continued on next page)

Continued

REAGENT or RESOURCE	SOURCE	IDENTIFIER
Software and algorithms		
Compass for Simple Western	Protein simple	N/A
IncuCyte analysis software	Sartorius	N/A
Cell profiler 3.0	CellProfiler	N/A
CASAVA v1.8.2	Illumina	N/A
MaxQuant 1.5.5.2	MaxQuant	N/A
Perseus v1.5.5.5	MaxQuant	N/A
Other		
SpectraMax i3	Molecular Devices	N/A
Neon Transfection System	Invitrogen	MPK5000
Wes	Bio-Techne	N/A
Odyssey Scanner	LI-COR	N/A
IncuCyte	Sartorius	N/A
Observer Z1 epifluorescence microscope	Zeiss	N/A
Nansluodrop 2000 Spectrometer	Thermo Scientific	N/A
Tapestation 2200	Agilent	N/A
HiSeq1500	Illumina	N/A
Bioruptor	Diagenode	N/A
EASYnLC 1200 system	Thermo Fisher	N/A
Q Exactive HFX	Thermo Fisher	N/A

EXPERIMENTAL MODEL AND SUBJECT DETAILS

Monocyte for use or differentiation into macrophages were obtained from buffy coats from healthy donors according to protocols accepted by the institutional review board at the University of Bonn (local ethics votes Lfd. Nr. 075/14). Due to privacy restrictions age and sex of donors was not available and so not recorded.

METHOD DETAILS

Isolation and culturing of primary human macrophages
Human PBMCs were obtained from buffy coat by density gradient centrifugation in Ficoll–Paque PLUS (GE Healthcare). PBMCs were incubated at 4°C with magnetic microbeads conjugated to monoclonal anti-human CD14 Abs (Miltenyi Biotec) and isolated by positive magnetic selection according to manufacturer's instructions (Miltenyi Biotec). Primary human macrophages were generated through differentiation of CD14$^+$ monocytes with 500 U/mL of recombinant human GM-CSF (ImmunoTools) in RPMI 1640 medium (Life Technologies) containing 10% FBS (Thermo Fisher), 1% penicillin/streptomycin, 1 × GlutaMAX, and 1 × sodium pyruvate (both from Life Technologies) for 3 days. Human monocytes-derived macrophages (hMDM) were cultured in RPMI 1640 medium (Life Technologies) containing 10% FBS (Thermo Fisher), 1% penicillin/streptomycin, 1 × GlutaMAX, and 1 × sodium pyruvate.

Inflammasome stimulation
For inflammasome stimulation assays hMDM were incubated with LPS (1 ng/mL) and SCFAs (0.1–10 mM) for 16 h prior to harvesting. For nigericin and needletox stimulation hMDM were stimulated O/N with LPS (1 ng/mL) before stimulation on the following day with nigericin (8 μM) or needletox (Lfn-PrgI 10 ng/mL, PA 10 ng/mL) for 1.5 h prior to sample harvesting. For Figure S2C, the HDAC inhibitors and butyrate were added simultaneously to the hMDM along with LPS.

Measurement of cytokine secretion
1 x 10^5 hMDM/well were seeded in a 96-well plate in 100 μL. 50 μL of LPS and/or SCFAs (0.1–10 mM) were added simultaneously and the hMDM incubated for 16 h. 100 μL of cell-free supernatant was collected. The cytokine concentration was determined by HTRF or ELISA according to the manufacturer's instructions. For some measurements, Bio-Plex Pro Human Cytokine 27-plex Assay kit was used according to the manufacturer's instructions.

Caspase-8 activity assay

1.5×10^5 hMDM/well were seeded into white 96-well plate in 100 μL (Figure 5A), or 0.5×10^5 hMDM/well in 60ul (Figure 5I). 100 μL or 40ul of the indicated stimuli were added to the cells. Cells were incubated for 16 h, or 1.5 h for nigericin. Afterward, the plate was centrifuged for 5 min at 340 x g and supernatants were collected for the measurement of cytokines. The cells were washed once with PBS. Then 25 μL caspase-8 Glo assay buffer containing MG-312 were added to the cells immediately. After the samples were incubated for 30–60 min in dark, the luminescent signal was measured at 470 nm by a SpectraMax i3 system.

Lactate dehydrogenase (LDH) assay

To determine the cell viability of hMDM in response to the treatment with LPS and butyrate, the activity of released LDH in the supernatants were measured and quantified as an indicator of cell death. 1×10^5 hMDM were seeded into 96-well plates in 100 μL RPMI 1640 medium containing 0.1% FCS. Another 100 μL indicated stimuli were added to and cultured with the cells for 16 h, after which the plate was centrifugated for 5 min at 340 x g to remove non-adherent cells from the supernatants. Meanwhile, 200 μL 1 x lysis buffer provided by the kit (Pierce LDH cytotoxicity Assay) were used to lyse the control cells as positive control. Afterwards, 25 μL supernatants and 25 μL LDH assay buffer were transferred and mixed in a transparent 384-well plate and incubated for 30 min in the dark. Then the absorbance was measured at 490 nm and 680 nm by a SpectraMax i3 system.

Small interfering RNA (siRNA) electroporation in primary human macrophages

All the siRNA-mediated knockdown experiments in primary human macrophages were performed by electroporation using a Neon Transfection System (MPK5000; Invitrogen). Each reaction used $1.2–1.5 \times 10^6$ hMDM, which were mixed with 10 μL buffer R and 75 pmol (1.5 μL) siRNA. Subsequently, the samples were taken up using a 10 μL Neon Pipette Tip and electroporated with the following protocol: 1400 V, 20 ms, 2 pulses. The electroporated cells were cultured in 10% FCS RPMI medium without antibiotics for 3 days or overnight for the cFLIP knock down. For some of the siRNAs with low knockdown efficiency, cells had to be electroporated again at day 3 after the first electroporation and cultured in 10% FCS RPMI medium without antibiotics for another 2 days. $0.5–1 \times 10^6$ cells were lysed by 30 μL RIPA buffer containing cOmpleteTM EDTA-free protease inhibitor and phosphatase inhibitor to prepare the samples for the validation of siRNA-mediated knockdown efficiency by either Western blot or WES.

Cloning

CFLAR WT was cloned from addgene plasmid #82936 by PCR before using restriction enzyme digest and ligation to insert it into a lentiviral vector containing a murine phosphoglycerate kinase 1 (PGK) promoter, as well as a C-terminal T2A followed by a mCherry and a Puromycin selection cassette.

Lentiviral transduction of primary human macrophages

To produce the virus-containing supernatant 7×10^6 HEK293T cells were plated in complete DMEM in a 10 cm dish. After 16–24 h, HEK293T cells were transfected with either a lentiviral construct encoding the gene of interest (2 μg per well) or a vector encoding the Vpx-Vpr restriction factors[47] with the pPAX2 (1 μg well), and pMD2.G (100 ng/well) plasmids using PEI MAX (Polyscience, 24765-100). Cells were incubated at 37C, 5% CO2 for approximately 12 h, and then the media was exchanged with RPMI containing 30% HI-FBS, and cells were incubated for another 36 h. After 36 h, the viral supernatant was collected using a 10 mL Luer-lock syringe attached to a blunt 18G needle and then filtered using a 0.45 mm filter unit into a 50 mL falcon. LentiX-concentrator was added as per manufactures instructions and the supernatant incubated overnight at 4°C. The virus was collected by centrifugation (1500xg, 50min, 4°C) and resuspended in complete RPMI. The Vpx-Vpr virus was mixed with the virus containing the gene of interest at a ratio of 1:1, 8 μg/mL polybrene was then added and the virus diluted 1:7 in complete RPMI. hMDM were seeded for transduction the day prior to transduction in 96 well plates, 0.4×10^5 cells/well and adhered overnight. The virus containing media was added to the hMDM for approx. 14 h at 37°C, 5% CO2. Following incubation, the cells were collected by centrifugation, and the virus-containing medium was removed and replaced by complete RPMI. The experiment was performed 24 h post-transduction.

Cellular potassium quantification

Following treatment, the supernatant was removed from the hMDM, which were then washed 3x in potassium free balanced salt solution (125 mM NaCl, 5 mM N-methyl-glucamine chloride, 2 mM MgCl2, 1 mM CaCl2, 10 mM Glucose, 10 mM HEPES pH 7.4.) and lysed in 1 mL of ddH$_2$O. The cells were freeze thawed three times to lyse them, then the supernatant harvested and clarified by centrifugation. Potassium was measured from the clarified supernatant by ICP-MS.

Immunoblotting

Up to 1×10^6 cells were lysed using RIPA buffer (20 mM Tris-HCl pH 7.4, 150 mM NaCl, 1 mM EDTA, 1% Triton X-100, 10% glycerol, 0.1% SDS and 0.5% deoxycholate) supplemented with PhosSTOP and complete protease inhibitors (Roche). Cell lysates were clarified by centrifugation at 10,000 x g for 10 min, followed by the protein concentration quantification by BCA assay. Equal amounts of samples for immunoblotting in NuPAGE LDS sample buffer and reducing agent were always incubated at 85°C for 10 min before loading onto a 4–12% or 10% NuPAGE Bis-Tris gel. As a size marker, 3 μL of PageRulerTM Plus prestained protein ladder were loaded on each gel. Samples were separated under denaturing and reducing electrophoretic conditions at 150 V in MOPS or

MES buffer. Separated proteins were then transferred from the gel to an Immobilon-FL polyvinylidene difluoride (PVDF) membrane at 32 V for 1–1.5 h. Non-specific antibody binding to the membrane was blocked by incubation of the membrane with blocking buffer for at least 1 h at RT. Antibodies diluted in binding buffer were incubated with the blocked membrane overnight at 4°C. Membranes were washed three times with TBST and then incubated with the secondary antibody for 1 h at RT in binding buffer. Membranes were then washed twice in TBST and one last time in TBS before being developed on an Odyssey Scanner (LI-COR).

Simple Western assay on WesTM

Protein concentration of each sample was normalized using the BCA assay to 1–2 $\mu g/\mu L$. Four parts of the lysates were combined with one part of the 5x Fluorescent Master Mix containing a fluorescently labeled standard, DTT and Sample Buffer, and were denatured by incubation at 95°C for 5 min. The samples, a biotinylated ladder, the primary antibody, streptavidin-horseradish peroxidase (HRP), the secondary antibody, the chemiluminescent substrate, and wash buffer were loaded, as indicated by the manufacturer, into a microplate pre-filled with Split Running Buffer, Wash Buffer and 10x Sample Buffer. Samples were electrophoretically separated and detected in a 25-capillary cartridge (12–230 kDa) using the following protocol: 200 s loading time of the separation matrix, 15 s loading time of the stacking matrix, 9 s loading time of the sample, 25 min separation time of the sample at 375 V, 90 min incubation with the primary antibody and 30 min incubation with the secondary antibody. Results were analyzed with the Compass for Simple Western software.

Live cell imaging for cell death analysis

hMDM were used to determine cell viability by live cell imaging. 3.5×10^4 cells/well were seeded into a 96-well plate in RPMI 1640 medium containing rhGM-CSF (3.1 $\mu L/mL$). Diyo-1 (1:10,000), a live cell imaging dye, was also added. Cells were allowed to reattach for 4 h before addition of any compounds. Cell death analysis was performed after stimulating the cells with LPS (1 ng/mL) and butyrate (10 mM), alone or in combination, using the IncuCyte bioimaging platform, which is housed in a high humidity, 37°C, 5% CO_2 incubator. LPS (10 ng/mL) was added 3 h prior to addition of nigericin (10 μM) as a positive control. Four images were captured per well in the appropriate fluorescent channels and phase contrast every one or 2 h for 24 h. These images were analyzed using the IncuCyte analysis software. The fluorescent count/image was averaged between four images/well. This was used to yield the average cell count/image/well, demonstrating membrane-permeabilized cells in the case of Diyo-1. Each condition was measured in technical duplicates for each donor.

ASC speck imaging and quantitation

200 μL of 1×10^6/mL hMDM per well were seeded in 8-well ibidi slides. The cells were treated with medium, LPS (1 ng/mL) or butyrate (10 mM), alone or in combination, for 16 h, or primed with LPS (10 ng/mL, 3 h) prior to the addition of NLRP3 inflammasome activator Nigericin (10 μM, 1.5 h). Then, the cells were fixed with 200 μL 4% formaldehyde in PBS after 30 min incubation at room temperature, followed by two washes with 200 μL PBS. 100 μL of mixtures containing 10 μL human FcR blocking reagent and 90 μL permeabilization buffer were incubated with the cells for 10 min at 37°C. Afterward, the cells were stained with 4 μL of directly labeled anti-ASC-647 (1:25) and incubated overnight at 4°C in the dark. To wash out the extra antibodies, the cells were washed twice with 200 μL permeabilization buffer. Subsequently, 100 μL DNA dye Hoechst diluted by PBS (1:3000) were incubated with the cells for 10 min at room temperature in the dark, followed by two washes with 200 μL PBS to remove the remaining Hoechst solution. Finally, the cells were filled with 200 μL PBS and imaged by Observer Z1 epifluorescence microscope (ZEISS). The analysis of ASC specks was processed by counting the number of cells using Hoechst as a nuclear marker as well as the ASC 647 signal to count the specks to ultimately calculate the number of ASC specks per cell. This analysis was performed by using the image analyser software Cell profiler 3.0.

Gene expression analysis by quantitative PCR (qPCR)

1×10^6 hMDM were seeded in 12-well plate and incubated with indicated stimuli for 16 h, after which 350 μL RLT lysis buffer containing 1% (v/v) β-mercaptoethanol were used to lyse the cells at room temperature. RNA was isolated according to the manufacturer's instructions (RNeasy Mini Kit, Qiagen). Equal quantities of RNA (500–1000 ng) from each sample were reverse transcribed into cDNA using the SuperScript III Reverse Transcriptase and oligo $dT_{(18)}$ primers. The qPCR was performed on the QuantStudio 6 Flex real-time PCR system, and the relative expression of the target mRNA was analyzed using the $\Delta\Delta C_T$ method with HPRT as the reference mRNA. For primer sequences see key resources table.

RNA-sequencing

1×10^6 GM-MDMs were treated with NaCl (10 mM), SCFAs (acetate, propionate or butyrate; 10 mM) or TSA (0.5 μM) in the presence or absence of LPS (1 ng/mL) for 16 h and subsequently lysed in TRIZOL (Invitrogen) and total RNA was extracted using the RNeasy Mini Kit (Qiagen) according to the manufacturer's protocol. RNA was eluted in RNase-free water. The quality of the RNA was assessed by measuring the ratio of absorbance at 260 nm and 280 nm using a Nanodrop 2000 Spectrometer (Thermo Scientific) and by visualization of 28S and 18S band integrity on a Tapestation 2200 (Agilent). Total RNA was converted into libraries of double-stranded cDNA molecules as a template for high-throughput sequencing using the Illumina TruSeq RNA Sample Preparation Kit v2. Briefly, mRNA was purified from 100 to 500 ng of total RNA using poly-T oligo-attached magnetic beads. Fragmentation

was carried out using divalent cations under elevated temperature in Illumina proprietary fragmentation buffer. First strand cDNA was synthesized using random oligonucleotides and SuperScript II. Second strand cDNA synthesis was subsequently performed using DNA Polymerase I and RNase H. Remaining overhangs were converted into blunt ends via exonuclease/polymerase activities and enzymes were removed. After adenylation of 3′ends of DNA fragments, Illumina adaptor oligonucleotides were ligated to prepare for hybridization. DNA fragments with ligated adaptor molecules were selectively enriched using Illumina PCR primers in a 15 cycles PCR reaction. Size-selection and purification of cDNA fragments with preferentially 200 bp in insert length was performed using SPRIBeads (Beckman-Coulter). Size distribution of cDNA libraries was measured using the Agilent high sensitivity DNA assay on a Tapestation 2200 (Agilent). cDNA libraries were quantified using KAPA Library Quantification Kits (Kapa Biosystems). After cluster generation on a cBot, 75 bp single read sequencing was performed on a HiSeq1500 and de-multiplexed using CASAVA v1.8.2.

RNA-sequencing analysis

Pre-processing of RNA-Seq data was performed by a standardized and reproducible pipeline based on the Docker system (Docker image is available via docker hub, limesbonn/hisat2). Briefly, alignment to the human reference genome hg19 from UCSC was conducted by Hisat2 (Hisat2, 2.0.6) (Kim et al., 2015) using standard settings. The external gene names and Entrez gene IDs matching the original Ensembl gene IDs were obtained using The biomaRt package (v2.38.0) (Kinsella et al., 2011) and A DGEList object was created using the raw counts and gene annotation using the edgeR package (v3.24.0) (Robinson et al., 2009). Since genes with very low counts are not useful, only genes that had at least 10 reads in a worthwhile number of samples determined by the design matrix were kept. In addition, each kept gene is required to have at least 15 reads across all the samples. Filtering was performed using the filterByExpr function. Afterward, counts were normalised. The aim of normalisation is to remove systematic technical effects that occur in the data to ensure that technical bias has minimal impact on the results. Normalisation was done by using TMM method (Robinson and Oshlack, 2010) (weighted, trimmed mean of M-values) with the application of edgeR calcNormFactors function. In contrast to other procedures, where the proportion of each gene's reads is computed relative to the total number of reads and compared across all samples, here it is taken into account that different experimental conditions might express a diverse RNA repertoire and therefore might lead to not directly comparable proportions. To put it simply, normalisation is supposed to level the median of gene expression values across samples, assuming that the majority of genes are expressed at an equal level. After data normalisation and with the edgeR package v3.24.0, estimateDisp was used to estimate common dispersion and tagwise dispersion and transform the data for linear modeling. Multidimensional scaling (MDS) plot visualising the relationship between the samples were displayed with the batch-corrected data according to all the donors. For each comparison, differentially expressed genes (DEGs) were identified with a false discovery rate (FDR)-adjusted p-value <0.05. Differential expression analysis was also performed with DESeq (v. 1.34.0)[48] to ensure robustness, and for comparison with ChIP-seq results. Gene set enrichment analysis was performed using the camera function of the limma package v3.38 (Wu and Smyth, 2012) with the hallmark gene set collections from the Molecular Signatures Database v5.2 (Liberzon et al., 2015; Subramanian et al., 2005).

ChIP-seq

10×10^6 GM-MDMs were treated with butyrate (10 mM) in the presence or absence of LPS (1 ng/mL) for 6 h. They were cross-linked with 1% formaldehyde, lysed and sonicated in 1% Triton, 0.1% sodium deoxycholate, 0.5% SDS, 0.2 M NaCl, 10 mM Tris, pH 7.5, 10 mM EDTA, and 1X protease inhibitor cocktail. Sonication was performed in a Covaris M220 (75% PIP, 200 CPB, 7°C, 10% DF) for 15 min in lysis buffer with 0.5% SDS. Lysates were incubated with 4 μg of H3K27ac antibody (Abcam) overnight at 4°C. For normalization, 50 ng of *Drosophila* spike-in chromatin (53083, Active Motif) and 2 μg of spike-in antibody (61686, Active Motif) were added. Antibody-bound chromatin was pulled down with protein G Dynabeads. Samples were washed, RNase-treated and reverse cross-linked by incubation at 65°C in 1% SDS, 0.1 M NaHCO$_3$ and proteinase K. DNA was purified using ChIP DNA Clean & Concentrator Kit (Zymo). Libraries were prepared using the NEBNext Ultra DNA Library Prep kit (New England Biolabs).

ChIP-seq data processing

ChIP-seq libraries were sequenced along with input libraries as paired end 150bp reads. Reads were aligned to human genome hg38 and to fruit fly genome dm6 using Bowtie2 version 2.4.4 with '–very-sensitive' flag set and a minimum fragment length (-X flag) of 1000bp,[49] all other parameters set to default. Normalization based on spike-in chromatin was performed within each biological replicate as follows: scaling factors were calculated for each sample as the ratio of total uniquely aligned counts to Drosophila relative to the counts in the sample containing the least number of Drosophila counts, and reads were down-sampled according to this ratio. Quality of the ChIP-Seq libraries were assessed using ChIPQC. Duplicate reads were identified using Picard MarkDuplicates and excluded from the downstream analysis. Genome wide coverage tracks in bigwig format were generated using DeepTools bamCoverage (v. 3.3.1).[50] ChIP-Seq Peaks were identified by MACS2 (v. 2.2.5)[50] using input libraries as control. Average ChIP-seq signal around TSS and intergenic peaks (>5 kb from closest gene) were calculated and plotted with deepTools using bigwig files as input (v. 3.3.1, computeMatrix and plotProfile, respectively). To quantify H3K27ac signal at promoters, ChIP-seq reads were quantified at promoters (+-500 bp of transcription start site) of all genes previously analyzed by RNA-seq. Differential ChIP-signal between samples was analyzed with DESeq2 (v. 1.34.0),[48] omitting default normalization as ChIP-seq signal was already normalized by spike-in chromatin.

GSEA

GSEA was carried out using ranked gene lists based on RNA-seq expression (wald statistics from DESeq2 results) and on ChIP-seq signal (log2FC of ChIP-seq counts at gene promoters). GSEA software v. 4.2.2 was used with a 'classic' scoring scheme and MSigDB gene sets.[51]

Motif enrichment

Enrichment analyses of known transcription factor motifs were performed at promoters of up and downregulated genes in RNA-seq and at the 10% of promoters with highest and lowest H3K27ac increase. Homer's findMotifsGenome.pl program[52] was utilized, using in each case all other promoters as background and a region size of 400 bp, with all other parameters set as default.

Mass spectrometry-based proteomics (MS)

1.5×10^6 GM-MDMs were cultured in 1 mL RPMI 1640 medium in 12-well plates and challenged by indicated stimuli for 16 h. The cells were washed twice with PBS before lysing the cells with 200 μL SDS lysis buffer containing freshly added DTT. Cell lysates were collected into new Eppendorf tubes and boiled for 10 min. 800 μL pre-cooled acetone were mixed with the samples and then incubated overnight at −20°C. Subsequently, the samples were washed twice with 80% acetone after centrifugation (19,000 x g, 20 min, 4°C). The pellets at the bottom of tubes were dried for 15 min at room temperature and stored at −80°C.

Frozen samples were resuspended in 50 μL of digestion buffer containing 1% SDC, 10 mM TCEP, 55 mM CAA, 25 mM Tris (pH = 8) and boiled for 10 min to denature proteins. After sonication using a Bioruptor (Diagenode), protein concentration was measured via BCA assay. 50 μg of proteins were digested with 1 μg Lys-C and Trypsin overnight at 37°C and 1500 rpm. Peptides were desalted and purified using 2 discs of SDB-RPS material and re-suspended in 2% acetonitrile/0.1% TFA for LC-MS.

Reverse phase chromatographic separation of peptides was performed by loading approximately 200–500 ng of peptides on a 50-cm HPLC-column (75-μm inner diameter; in-house packed using ReproSil-Pur C18-AQ 1.9-μm silica beads; Dr Maisch GmbH, Germany) coupled to an EASYnLC 1200 ultra-high-pressure system Peptides were separated with a buffer system consisting of 0.1% formic acid (buffer A) and 80% acetonitrile in 0.1% formic acid (buffer B) using a linear gradient from 5 to 30% B in 110 min. The column temperature was set to 60°C.

The LC was coupled to a quadrupole Orbitrap mass spectrometer (Q Exactive HFX, Thermo Fisher Scientific, Rockford, IL, USA) via a nano-electrospray ion source. The mass spectrometer was operated in a data-dependent acquisition mode, collecting MS1 spectra (60,000 resolution, 300–1650 m/z range) with an automatic gain control (AGC) target of 3E6 and a maximum ion injection time of 20 m. The top-15 most intense ions from the MS1 scan were isolated with an isolation width of 1.4 m/z. Following higher-energy collisional dissociation (HCD) with a normalized collision energy (NCE) of 27%, MS2 spectra were collected (15,000 resolution) with an AGC target of 5E4 and a maximum ion injection time of 28 m. Dynamic precursor exclusion was enabled with a duration of 30 s.

MS data processing and analysis

Mass spectra were searched against the 2019 Uniprot mouse databases using MaxQuant version 1.5.5.2 with a 1% FDR at the peptide and protein level. Peptides required a minimum length of seven amino acids with carbamidomethylation as a fixed modification, and N-terminal acetylation and methionine oxidations as variable modifications. Enzyme specificity was set as C-terminal to arginine and lysine using trypsin as protease and a maximum of two missed cleavages were allowed in the database search. The maximum mass tolerance for precursor and fragment ions was 4.5 ppm and 20 ppm, respectively. 'Match between runs' was enabled to transfer peptide identifications between individual measurements with a 0.7-min window after retention time alignment. Label-free quantification was performed with the MaxLFQ algorithm using a minimum ratio count of 2. Protein identifications were filtered by removing matches to the reverse database, matches only identified by site, and common contaminants. Data filtering and Statistical analysis was performed with Perseus v1.5.5.5, GraphPad Prism v7.03, Microsoft Excel, and R Studio v3.4.0. Data was filtered further such that only proteins with identifications in all replicates of one cell type were retained. Missing values were imputed from a normal distribution of intensity values at the detection limit of the mass spectrometer. Statistical analysis was performed as indicated in the Figure legends with a constant permutation-based FDR correction at 5%.

QUANTIFICATION AND STATISTICAL ANALYSIS

Data analysis and statistical analysis was performed in R and GraphPad Prism. All statistical analysis were preceded by Normality tests, followed by parametric tests as all data was found to be normal. The 'n' represents the number of unique donors that experiment was performed with. p values were determined by two-way ANOVA with Tukey's or Sidak's tests. Values of $p < 0.05$ were considered statistically significant. $*p < 0.05$, $**p < 0.01$, $***p < 0.0002$, $****p < 0.0001$. Data are graphed as mean; error bars show SEM unless otherwise stated.